
How Inductive Bias in Machine Learning Aligns with Optimality in Economic Dynamics

Mahdi Ebrahimi Kahou¹ James Yu² Jesse Perla² Geoff Pleiss^{2,3}

¹Bowdoin College ²University of British Columbia ³Vector Institute

m.ebrahimikahou@bowdoin.edu

yuyuming@student.ubc.ca

jesse.perla@ubc.ca

geoff.pleiss@stat.ubc.ca

Abstract

This paper examines the alignment of inductive biases in machine learning (ML) with structural models of economic dynamics. Unlike dynamical systems found in physical and life sciences, economics models are often specified by differential equations with a mixture of easy-to-enforce initial conditions and hard-to-enforce infinite horizon boundary conditions (e.g. transversality and no-ponzi-scheme conditions). Traditional methods for enforcing these constraints are computationally expensive and unstable. We investigate algorithms where those infinite horizon constraints are ignored, simply training unregularized kernel machines and neural networks to obey the differential equations. Despite the inherent underspecification of this approach, our findings reveal that the inductive biases of these ML models innately enforce the infinite-horizon conditions necessary for the well-posedness. We theoretically demonstrate that (approximate or exact) min-norm ML solutions to interpolation problems are sufficient conditions for these infinite-horizon boundary conditions in a wide class of problems. We then provide empirical evidence that deep learning and ridgeless kernel methods are not only theoretically sound with respect to economic assumptions, but may even dominate classic algorithms in low to medium dimensions. More importantly, these results give confidence that, despite solving seemingly ill-posed problems, there are reasons to trust the plethora of black-box ML algorithms used by economists to solve previously intractable, high-dimensional dynamical systems—paving the way for future work on estimation of inverse problems with embedded optimal control problems.

1 Introduction

Numerical solutions to dynamical systems are central to many quantitative fields in economics, including macroeconomics, finance, international trade, labor, and industrial organization. For example, a model of capital accumulation and consumption consists of a differential (or difference) equation enforcing market dynamics, an initial condition defining the starting capital, and intra-temporal conditions ensuring that supply and demand are balanced. Statistical models of these economic processes are used as laboratories for counterfactual scenarios, such as evaluating the impact of changes in capital gains tax rates on investment. Economists are increasingly interested in applying ML techniques towards forward and inverse modeling of these systems, motivated by remarkable successes on dynamical systems in physical and life sciences [e.g. 10, 13, 27, 39].

Challenges of economic dynamical systems. ML techniques for forward and inverse modeling typically target initial-value problems (IVP) that are entirely specified by the differential equation

and initial conditions on all variables.¹ In contrast, economic systems often embed infinite-horizon optimal control problems which include *asymptotic boundary conditions* (e.g. transversality and no-ponzi-scheme conditions)—presenting challengers to both classical and ML algorithms.

The asymptotic boundary conditions are necessary to ensure the problem is *well-posed* in the sense of Hadamard (i.e., a solution exists, is unique, and changes smoothly with initial conditions).² In particular, without imposing these asymptotic boundary conditions there will be a continuum of solutions which fulfill the initial conditions and ODEs. Classical methods to solve these problems and apply the asymptotic boundary conditions are often numerically unstable and shooting towards steady states of the system—which adds numerical instability, and unique challenges when there is *steady-state multiplicity* and hysteresis (i.e., requirements to partition the space into different basins of attraction for each steady state).

Despite these challenges, economists are putting their faith in standard ML methods for forward and inverse modeling with applications ranging from wealth inequality [24], financial frictions coupled with inequality [20], the heterogeneous impacts of climate change [4], portfolio choice problems [2], heterogeneous agent new Keynesian models [26], human capital accumulation in the labor market [25], and labor market dynamics in search and matching [36]—using neural networks [3, 17, 18, 30] or kernel machines [38]. However, while these methods encode initial values, they *simply ignore the asymptotic boundary conditions* and solve the underspecified, *ill-posed* problems—so there are no guarantees on which solution the ML model will find.

Inductive bias of machine learning. In this paper, we investigate to what extent the *implicit biases* of these ML models will automatically fulfill the asymptotic boundary conditions of economic systems—despite solving an ill-posed problem. Large neural networks or ridgeless kernel regressors can learn to satisfy a system of differential equations on any amount of data/grid points, thus implying that these models are *overparameterized*. Recent work in optimization suggests that SGD-based training of these overparameterized models will (approximately) yield the minimum-norm function capable of interpolating the data [5]. In the case of dynamical systems modeling, this implies that neural networks and kernel machines will find the minimum-norm function that (locally) satisfies the dynamical system and whatever explicit constraints are known. Put differently, ML models of economic dynamical systems with minimum function norm constraints may provide sufficient conditions for the asymptotic boundary-value constraints.

This leads to our key research question: does the minimum norm inductive bias of machine learning align with asymptotic constraints of economics models? Outside of general appeals to Occam’s Razor, there is no reason that these two should align.

Contributions. We provide guidance on when and why we can trust ML solutions for an important class of dynamical systems used in economics. In particular, we show:

- **inductive bias alignment:** theoretical and empirical evidence that the minimum norm implicit bias of large machine learning models aligns with many asymptotic boundary conditions found in economics problems;
- **learning the right set of steady-states:** evidence that kernel machines and neural networks find the optimal steady states of dynamical systems—leading to very accurate generalization outside of the training data—even without enforcing asymptotic boundary conditions;
- **consistency of ML estimates:** guarantees that ML methods converge to the true minimum-norm solutions (and thus, in many cases, the asymptotic boundary constrained solutions) in the limit of infinite data; and
- **robustness and speed:** demonstrations that kernel machines and neural networks may be competitive in speed and robustness with traditional methods for modeling economic systems, even on small-scale problems.

¹In some cases, mixed with terminal boundary values at a finite-horizon (e.g., [23], [41], and [35] for theory on the role of terminal, *finite horizon* boundary conditions).

²The definition of “well-posed” used here can be traced back to Hadamard’s works [21, 22]. Also, see [43] and [49] for classic treatments of regularization to solve *ill-posed* problems, of which our methods are broadly connected.

Finally, this lays the foundation for future work on solving inverse problems that will jointly estimate structural parameters and solve dynamic models (in contrast to approaches like [15], which require solving a dynamical system through standard techniques as a nested step in forming the likelihood).

2 Setup

The economic systems we are concerned with have roots in optimal control theory, though many will contain additional algebraic constraints not found in classical optimal control setups. An inherent characteristic of infinite-horizon optimal control problems, whether deterministic or stochastic, are asymptotic boundary conditions such as transversality conditions. These conditions can be formulated sequentially or recursively in a state space, and in continuous- or discrete-time (see discussions of necessary conditions in [6, 32, 44]). In this paper, we will focus on an important subset of these problems—deterministic, continuous-time systems of differential-algebraic equations (DAE)—which allow for formal proof of results and comparison to baseline solutions from preexisting algorithms.

Problem class. Within the subset of problems we formally analyze here, classic nonlinear optimal control decisions are embedded in a large class of economic problems, resulting in systems of ordinary differential and algebraic equations [1]. Partitioning these into three vectors: *state variables* $\mathbf{x}(t) \in \mathbb{R}^{M_x}$ with an initial condition \mathbf{x}_0 ; *jump variables* $\mathbf{y}(t) \in \mathbb{R}^{M_y}$ with accompanying asymptotic boundary conditions typically from the embedded control problems; and optional *static variables* $\mathbf{z}(t) \in \mathbb{R}^{M_z}$.³ Given this, the dynamical system with primitives $\mathbf{F}, \mathbf{G}, \mathbf{H}, \mathbf{B}$ is

$$\dot{\mathbf{x}}(t) = \mathbf{F}(\mathbf{x}(t), \mathbf{y}(t), \mathbf{z}(t)) \quad (1)$$

$$\dot{\mathbf{y}}(t) = \mathbf{G}(\mathbf{x}(t), \mathbf{y}(t), \mathbf{z}(t)) \quad (2)$$

$$\mathbf{0} = \mathbf{H}(\mathbf{x}(t), \mathbf{y}(t), \mathbf{z}(t)) \quad (3)$$

subject to an initial value $\mathbf{x}(0) = \mathbf{x}_0$ and boundary conditions

$$\mathbf{0} = \lim_{t \rightarrow \infty} \mathbf{B}(t, \mathbf{x}(t), \mathbf{y}(t), \mathbf{z}(t)) \quad (4)$$

Key necessary conditions to be *well-posed* are that \mathbf{x}_0 is given, there exists a $\mathbf{y}(0)$ uniquely determined using the asymptotic boundary condition Eq. (4), and—where applicable—there exists a unique $\mathbf{z}(0)$ fulfilling Eq. (3) given $\mathbf{y}(0)$.⁴

Algorithmic challenges with classic, non-ML methods. Since this problem looks deceptively standard, it is worth emphasizing the challenges before explaining how ML algorithms can tackle them. If an initial condition for $\mathbf{y}(0)$ was given, then Eqs. (1) and (2) is an initial value problem (IVP) ODE which is well-posed and can be solved with high dimensional $\mathbf{x}(t)$ and $\mathbf{y}(t)$ using a variety of classical methods.⁵ The central challenge to this class of problems is that applying Eq. (4) numerically is not directly possible, as it is asymptotic, and approximations to learn $\mathbf{y}(0)$ are numerically unstable since the solution path lies on a saddle-path (see [1]). These problems are compounded when there is steady-state multiplicity (i.e., regions of initial conditions x_0 which converge to separated x_∞). Central to our algorithm in Sec. 3 is the insight that the least-explosive solutions to the under-determined system Eqs. (1) to (3) given $\mathbf{x}(0) = \mathbf{x}_0$ initial condition will be those that fulfill Eq. (4).

3 Method

In this paper we use a machine learning approach for forward modeling of the dynamical system described in Sec. 2. Specifically, we will train large machine learning models to learn functions $\hat{\mathbf{x}}$,

³When required, static variables constrain the solution manifold and are not matched with boundary or initial values. The connection between the number of *jump variables* and stability local to a steady-state is discussed in [7].

⁴We will assume sufficient regularity conditions to make this possible, such as Lipschitz \mathbf{F}, \mathbf{G} and \mathbf{H} , and that $\det(\nabla \mathbf{H}) \neq 0$.

⁵The optional DAE term with $\mathbf{z}(t)$ and Eq. (3) adds additional, but surmountable, challenges for IVPs.

$\hat{\mathbf{y}}, \hat{\mathbf{z}}$ that minimize the following objective function:

$$\min_{\hat{\mathbf{x}}, \hat{\mathbf{y}}, \hat{\mathbf{z}}} \sum_{t_i \in \mathcal{D}} \left[\eta_1 \left\| \hat{\mathbf{x}}(t_i) - \mathbf{F}(\hat{\mathbf{x}}(t_i), \hat{\mathbf{y}}(t_i), \hat{\mathbf{z}}(t_i)) \right\|_2^2 + \eta_2 \left\| \hat{\mathbf{y}}(t_i) - \mathbf{G}(\hat{\mathbf{x}}(t_i), \hat{\mathbf{y}}(t_i), \hat{\mathbf{z}}(t_i)) \right\|_2^2 + \eta_3 \left\| \mathbf{H}(\hat{\mathbf{x}}(t_i), \hat{\mathbf{y}}(t_i), \hat{\mathbf{z}}(t_i)) \right\|_2^2 + \eta_4 \left\| \hat{\mathbf{x}}(0) - \mathbf{x}_0 \right\|_2^2 \right], \quad (5)$$

where \mathcal{D} is a set of time points from some fixed interval $[0, T]$. At first glance, there are several potential problems with this approach. Most critically, Eq. (5) completely ignores the asymptotic boundary condition in Eq. (4). The resulting learning problem is thus ill-posed. Despite this under-specification, we will show that many overparameterized ML models trained with gradient descent tend towards economically-optimal solutions—i.e. those that (approximately) satisfy Eq. (4). These results justify the use of ML models for solving economic models with embedded optimal control problems and also hint at scalability and numerical benefits over classic algorithms.

Intuition: overparameterized ML models tend towards minimum norm solutions. Overparameterized models by definition have more parameters than training data points, and thus there are many settings of parameters capable of “interpolating” (perfectly fitting) the training data. Recent work has suggested that overparameterized models in ML tend towards the interpolating solution with the smallest norm in the hypothesis class [e.g. 5]. This property is exactly true for linear models like kernel machines, and many SGD-trained neural networks are implicitly regularized towards small-norm solutions [29]. We will see that—with careful design—this minimum-norm inductive bias can be used as an approximate stand-in for the infinite-horizon boundary condition in Eq. (4).

Goal: minimum Sobolev seminorm solutions. In particular, we will use overparameterized ML models for Eq. (5) that are biased towards minimum *Sobolev seminorm* interpolating solutions. Given a function $w : [0, \infty) \rightarrow \mathbb{R}$ from $\mathcal{W}^{P+1,2}(\mathbb{R}^+)$, the Sobolev- $P+1, 2$ seminorm of w is defined as the Sobolev- $P, 2$ norm of its weak derivative: $|w|_{\mathcal{W}^{P+1,2}(\mathbb{R}^+)} := \|\dot{w}\|_{\mathcal{W}^{P,2}(\mathbb{R}^+)}$. The minimal structure required for many economic models is that will have a single derivative almost everywhere, and hence we can assume solutions to our problem classes lie in Sobolev spaces. From a theoretical perspective, there is an established connection between infinite-horizon optimal solutions of economic growth models and Sobolev spaces [44] and [14]. (In Sec. 4.1 we explore an economic model where the minimum Sobolev seminorm solution provably coincides with infinite-horizon boundary conditions.) More intuitively, a Sobolev seminorm bias is a natural choice to resolve the instability issues of classic algorithms. Solutions to Eqs. (1) to (3) either diverge, in which case $\dot{\mathbf{x}}(t)$ or $\dot{\mathbf{y}}(t)$ are large in absolute value, or they convergence and fulfil Eq. (4). Hence, $\|\dot{\mathbf{x}}\|_{L_2(\mathbb{R}^+)} = |\mathbf{x}|_{\mathcal{W}^{1,2}(\mathbb{R}^+)}$ would be large for instable/incorrect solutions and small for stable/correct solutions.

The inductive bias of ridgeless kernel regression. Our first ML model class that we consider is ridgeless kernel regression. This model class has the advantage that we can formally characterize the function norms and underlying inductive bias. Specifically, we represent $\hat{\mathbf{x}}, \hat{\mathbf{y}}, \hat{\mathbf{z}}$ as

$$\begin{aligned} \hat{\mathbf{x}}(t) &= \mathbf{x}_0 + \int_0^t \hat{\mathbf{x}}(\tau) d\tau, & \hat{\mathbf{y}}(t) &= \hat{\mathbf{y}}_0 + \int_0^t \hat{\mathbf{y}}(\tau) d\tau, & \hat{\mathbf{z}}(t) &= \hat{\mathbf{z}}_0 + \int_0^t \hat{\mathbf{z}}(\tau) d\tau, \\ \dot{\hat{\mathbf{x}}}(t) &= \sum_{j=1}^N \alpha_j^x K(t, t_j), & \dot{\hat{\mathbf{y}}}(t) &= \sum_{j=1}^N \alpha_j^y K(t, t_j), & \dot{\hat{\mathbf{z}}}(t) &= \sum_{j=1}^N \alpha_j^z K(t, t_j), \end{aligned} \quad (6)$$

where $\alpha_j^x, \alpha_j^y, \alpha_j^z, \hat{\mathbf{y}}_0, \hat{\mathbf{z}}_0$ are learned parameters and $K(\cdot, \cdot)$ is the Matérn kernel with smoothness ν and lengthscale ℓ . As we will demonstrate shortly, it is necessary to model $\dot{\hat{\mathbf{x}}}, \dot{\hat{\mathbf{y}}}, \dot{\hat{\mathbf{z}}}$ rather than $\hat{\mathbf{x}}, \hat{\mathbf{y}}, \hat{\mathbf{z}}$ to target the Sobolev seminorm rather than the Sobolev norm.

If we add an infinitesimal $\sum_{i,j=1}^N \alpha_i^x \alpha_j^x K(t_i, t_j)$ regularization term to the objective function in Eq. (5) (and analogous terms for y and z), then the solution to the optimization problem will be infinitesimally close to the minimum-norm solution:

$$\begin{aligned} \min_{\substack{\hat{\mathbf{x}} \in \mathcal{H}^{M_x}, \hat{\mathbf{y}} \in \mathcal{H}^{M_y}, \hat{\mathbf{z}} \in \mathcal{H}^{M_z} \\ \dot{\mathbf{y}}_0 \in \mathbb{R}^{M_y}, \dot{\mathbf{z}}_0 \in \mathbb{R}^{M_z}}} & \left(\sum_{m=1}^{N_x} \|\dot{\hat{\mathbf{x}}}^{(m)}\|_{\mathcal{H}}^2 + \sum_{m=1}^{N_y} \|\dot{\hat{\mathbf{y}}}^{(m)}\|_{\mathcal{H}}^2 + \sum_{m=1}^{N_z} \|\dot{\hat{\mathbf{z}}}^{(m)}\|_{\mathcal{H}}^2 \right) \quad (7) \\ \text{s.t. } & \dot{\hat{\mathbf{x}}}(t_i) = \mathbf{F}(\hat{\mathbf{x}}(t_i), \hat{\mathbf{y}}(t_i), \hat{\mathbf{z}}(t_i)), \quad \text{for all } t_i \in \mathcal{D} \\ & \dot{\hat{\mathbf{y}}}(t_i) = \mathbf{G}(\hat{\mathbf{x}}(t_i), \hat{\mathbf{y}}(t_i), \hat{\mathbf{z}}(t_i)), \quad \text{for all } t_i \in \mathcal{D} \\ & \mathbf{0} = \mathbf{H}(\hat{\mathbf{x}}(t_i), \hat{\mathbf{y}}(t_i), \hat{\mathbf{z}}(t_i)), \quad \text{for all } t_i \in \mathcal{D} \end{aligned}$$

where $\|\cdot\|_{\mathcal{H}}$ denotes the RKHS norm associated with the Matérn kernel. For functions defined over compact domains, it is well established that the Matérn RKHS with $\nu = (P - 1/2)$ and a specific value of ℓ is exactly equal to the $\mathcal{W}^{P,2}([0, T])$ norm for all $P \geq 1$ (see Appx. A). Thus, the Matérn kernel with $\nu = 1/2$ (and appropriate lengthscale) produces the minimum $\mathcal{W}^{2,2}([0, T])$ -seminorm solution. While this does not perfectly align with the $\mathcal{W}^{1,2}(\mathbb{R}^+)$ seminorm of interest,⁶ we experimentally demonstrate in Sec. 4 that minimum $\mathcal{W}^{2,2}([0, T])$ solutions closely align with those that satisfy Eq. (4).

Finally, we prove that $\hat{\mathbf{x}}, \hat{\mathbf{y}}, \hat{\mathbf{z}}$ are consistent estimators of the true minimum $\mathcal{W}^{2,2}([0, T])$ -seminorm solution to Eqs. (1) to (3). (See Appx. B for the proof.)

Theorem 1. *Given some $0 < K < \infty$, let \mathbb{S} be the set of functions $(\mathbf{x}, \mathbf{y}, \mathbf{z})$ that satisfy Eqs. (1) to (3) with $\mathbf{x}(0) = \mathbf{x}_0$ and $\|\mathbf{y}(0)\|_{\infty}, \|\mathbf{z}(0)\|_{\infty} \leq K$. If*

- $t \in \mathcal{D}$ are drawn uniformly i.i.d. from $[0, T]$;
- \mathbf{F}, \mathbf{G} , and \mathbf{H} in Eqs. (1) to (3) are Lipschitz with respect to $\|\cdot\|_{\infty}$; and
- \mathbf{F} and \mathbf{G} have Lipschitz first derivatives and \mathbf{H} has Lipschitz first and second derivatives,

then then the solutions $\hat{\mathbf{x}}_N, \hat{\mathbf{y}}_N, \hat{\mathbf{z}}_N$ from Eq. (7) with the Matern-1/2 kernel satisfies Eqs. (1) to (3) almost everywhere in the limit as $N \rightarrow \infty$ and

$$\lim_{N \rightarrow \infty} \sum_{m=1}^{M_x} |\hat{\mathbf{x}}_N^{(m)}|_{\mathcal{W}^{2,2}([0, T])}^2 + \sum_{m=1}^{M_y} |\hat{\mathbf{y}}_N^{(m)}|_{\mathcal{W}^{2,2}([0, T])}^2 + \sum_{m=1}^{M_z} |\hat{\mathbf{z}}_N^{(m)}|_{\mathcal{W}^{2,2}([0, T])}^2 \\ \stackrel{\text{a.s.}}{=} \inf_{(\mathbf{x}, \mathbf{y}, \mathbf{z}) \in \mathbb{S}} \sum_{m=1}^{M_x} |\hat{\mathbf{x}}^{(m)}|_{\mathcal{W}^{2,2}([0, T])}^2 + \sum_{m=1}^{M_y} |\hat{\mathbf{y}}^{(m)}|_{\mathcal{W}^{2,2}([0, T])}^2 + \sum_{m=1}^{M_z} |\hat{\mathbf{z}}^{(m)}|_{\mathcal{W}^{2,2}([0, T])}^2.$$

The inductive bias of neural networks. Alternatively, we consider solutions to Eq. (5) where $\hat{\mathbf{x}}, \hat{\mathbf{y}}, \hat{\mathbf{z}}$ are represented by overparameterized neural networks trained with stochastic gradient descent. While the inductive bias of neural networks is difficult to formally characterize, recent work suggests that they are approximately biased towards minimum Sobolev seminorm solutions. For infinite width neural networks, the inductive bias is towards the minimum norm solution in the RKHS of the neural tangent kernel [5]. For finite width neural networks, the implicit bias of SGD regularizes the Sobolev seminorm of the solution [29]. We empirically demonstrate in Sec. 4 that neural networks, like ridgeless kernel regression, recover solutions that satisfy Eq. (4).

4 Results

We solve two standard baselines in dynamic economics: a model of risk-neutral asset pricing (Sec. 4.1) and the neoclassical growth model (Sec. 4.2). These problems are chosen because they are standard examples in textbooks [e.g. 28], they admit reference solutions from classical methods, and they have established results regarding the set of solutions to the ill-posed versions without the asymptotic boundary conditions.⁷ In Sec. 4.3, we show a case where multiple steady states exist—a setting where our methods are especially helpful—and summarize other experiments in Sec. 4.4.⁸

For both baseline examples, we compare two ML methods trained on $\mathcal{D} := \{0, 1, 2, \dots, 30\}$:

Neural networks. We model $\hat{\mathbf{x}}(t)$ and $\hat{\mathbf{y}}(t)$ (and $\hat{\mathbf{z}}(t)$ when applicable) with overparameterized neural networks and minimize Eq. (5) directly. Crucially, there is no explicit regularization and Eq. (3) is not imposed directly, so this model relies exclusively on the inductive bias of the optimization process to align with the economically-optimal solution.

⁶Note that we cannot target the Sobolev-1, 2 seminorm with Eq. (6), as $|w|_{\mathcal{W}^{1,2}} = \|\dot{w}\|_{L_2}$ and L_2 is not an RKHS. Moreover, we cannot target Sobolev spaces of $[0, \infty)$ functions as the Matérn kernel only provably aligns with Sobolev spaces over functions with Lipschitz boundaries (see Appx. A).

⁷For asset pricing models, see [8, 16], which characterizes the set of solutions not fulfilling transversality and connects them to economic bubbles. [1] covers saddle-path analysis of the neoclassical growth model as a way to analyze failures of the transversality condition.

⁸In our baseline examples, the models have been simplified to eliminate static variables (i.e., no $\hat{\mathbf{z}}(t)$), but examples of the broader problem class are discussed in Sec. 4.4.

Matérn kernels. We solve with the kernel approximation in Eq. (7), which directly minimizes the function norm in the RKHS. We use the Matérn kernel with $\nu = 1/2$ to align with the $\mathcal{W}^{2,2}([0, T])$ seminorm, which is “close” to the $\mathcal{W}^{1,2}(\mathbb{R}^+)$ seminorm of interest.

4.1 Asset Pricing

Models of asset pricing and “rational bubbles” are relatively simple and benefit from closed-form solutions. These models have traditionally served a pedagogical role in demonstrating the necessity of transversality conditions; for instance, see [28]. The model values a sequence of dividends where, in cases of deviation from the fundamentals, the asset price reflects a “bubble.” Let $\mathbf{x}(t) \in \mathbb{R}$ be the flow payoffs from a claim to an asset, and $\mathbf{y}(t) \in \mathbb{R}$ be the price of a claim to that asset. For simplicity, we assume that the flow payoffs, \mathbf{x} , follow a deterministic process. For a given x_0 , the key equations are⁹

$$\dot{\mathbf{x}}(t) = c + g\mathbf{x}(t) := \mathbf{F}(\mathbf{x}(t), \mathbf{y}(t)) \quad (8)$$

$$\dot{\mathbf{y}}(t) = r\mathbf{y}(t) - \mathbf{x}(t) := \mathbf{G}(\mathbf{x}(t), \mathbf{y}(t)) \quad (9)$$

$$0 = \lim_{t \rightarrow \infty} e^{-rt} \mathbf{y}(t) := \mathbf{B}(\mathbf{x}(t), \mathbf{y}(t)) \quad (10)$$

where constants c, g govern the process for dividends and $r > 0$ is a risk-neutral investor’s discount rate. Eq. (10) is called a “no-bubble” condition in this case. The set of solutions to Eqs. (8) and (9), without imposing Eq. (10), can be found analytically (see [16, 28]):

$$\mathbf{y}(t) = \int_0^\infty e^{-r\tau} \mathbf{x}(t + \tau) d\tau = \mathbf{y}_f(t) + \zeta e^{rt}, \quad (11)$$

$$\mathbf{y}_f(t) := \frac{c}{r-g} + \left(x_0 - \frac{c}{r-g} \right) e^{(r-g)t} \quad (12)$$

where $\mathbf{y}_f(t)$ is interpreted as the “fundamental” price of the asset, and $\zeta \geq 0$ is indeterminate. However, when the “no-bubble” condition (i.e., Eq. (10)) is imposed, this problem is well-posed, with a unique solution of $\mathbf{y}(t) = \mathbf{y}_f(t)$ (i.e., $\zeta = 0$).

Sufficiency of the min-norm solutions to select the “no-bubble” solution. A key property of this example is that Eq. (11) characterizes the full set of solutions to Eqs. (8) and (9) when not imposing Eq. (10). For a given function norm, apply the triangle inequality to the set of solutions from Eq. (11) to yield $\|\mathbf{y}_f\|_{\mathcal{H}} \leq \|\mathbf{y}\|_{\mathcal{H}} \leq \|\mathbf{y}_f\|_{\mathcal{H}} + \zeta \|e^{rt}\|$. This shows that among the possible solutions to the ill-posed problem, the norm $\|\mathbf{y}\|_{\mathcal{H}}$ is minimized when $\zeta = 0$, at which point $\mathbf{y}(t) = \mathbf{y}_f(t)$ and the “no-bubble” condition in Eq. (10) is fulfilled.

Results. Fig. 1 shows the results of the kernel machine and neural network approximations.¹⁰ Despite not applying the “no-bubble” condition in Eq. (10), both the kernel interpolator and the neural network recover the unique equilibrium of economic interest almost perfectly.

4.2 Neoclassical Growth Model

The neoclassical growth model (also known as the Ramsey–Cass–Koopman model) is the benchmark problem in macroeconomics to explore optimal control in dynamical systems (see [1] for its many variations). A planner optimizes paths of capital, $\mathbf{x}(t) \in \mathbb{R}$, and consumption $\mathbf{y}(t) \in \mathbb{R}$, given an initial condition $x(0) = x_0$. Key parameters are a depreciation rate $\delta > 0$, discount rate $r > 0$, and a production function $f(x) := x^a$ where a is the capital share of output.¹¹

$$\dot{\mathbf{x}}(t) = f(\mathbf{x}(t)) - \mathbf{y}(t) - \delta \mathbf{x}(t) := \mathbf{F}(\mathbf{x}(t), \mathbf{y}(t)) \quad (13)$$

$$\dot{\mathbf{y}}(t) = \mathbf{y}(t) [f'(\mathbf{y}(t)) - \delta - r] := \mathbf{G}(\mathbf{x}(t), \mathbf{y}(t)) \quad (14)$$

$$0 = \lim_{t \rightarrow \infty} e^{-rt} \mathbf{x}(t)/\mathbf{y}(t) := \mathbf{B}(\mathbf{x}(t), \mathbf{y}(t)) \quad (15)$$

⁹Our baseline parameters are $x_0 = 1.0, c = 0.02, g = -0.2$, and $r = 0.1$.

¹⁰The neural network maps t to $\mathbf{y}(t)$. We use 4 hidden layers with 128 nodes and the Tanh activation function. In the final layer, the Softplus is used to ensure positive values for prices. For optimization, we use Adam with a learning rate of 10^{-3} .

¹¹Our baseline parameters are $x_0 = 1.0, \delta = 0.1, r = 0.11$, and $a = \frac{1}{3}$.

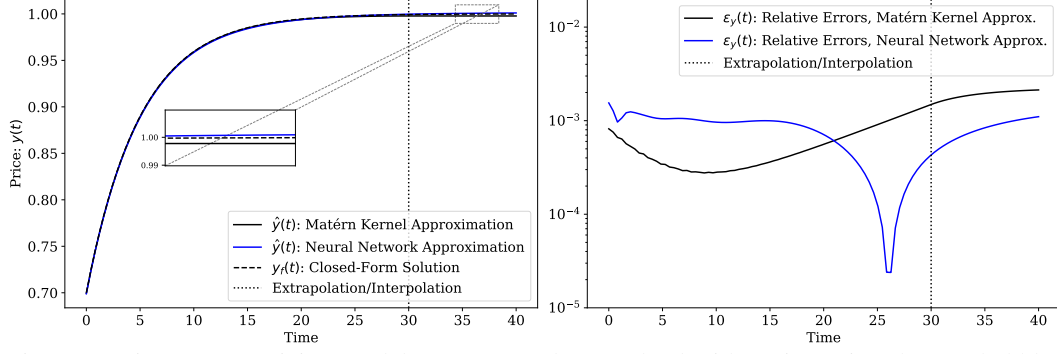


Figure 1: Linear asset pricing model (Eqs. (8) and (9)) solved without imposing the “no bubble” condition (Eq. (10)). The left panel shows the kernel machine and neural network approximations relative to the benchmark. The right panel displays the absolute errors relative to the benchmark on a test set of 100 points from $t = 0$ to $t = 40$. In all cases, the ML methods recover the benchmark and even extrapolate well beyond the training data, despite solving an indeterminate problem and not directly calculating the steady state.

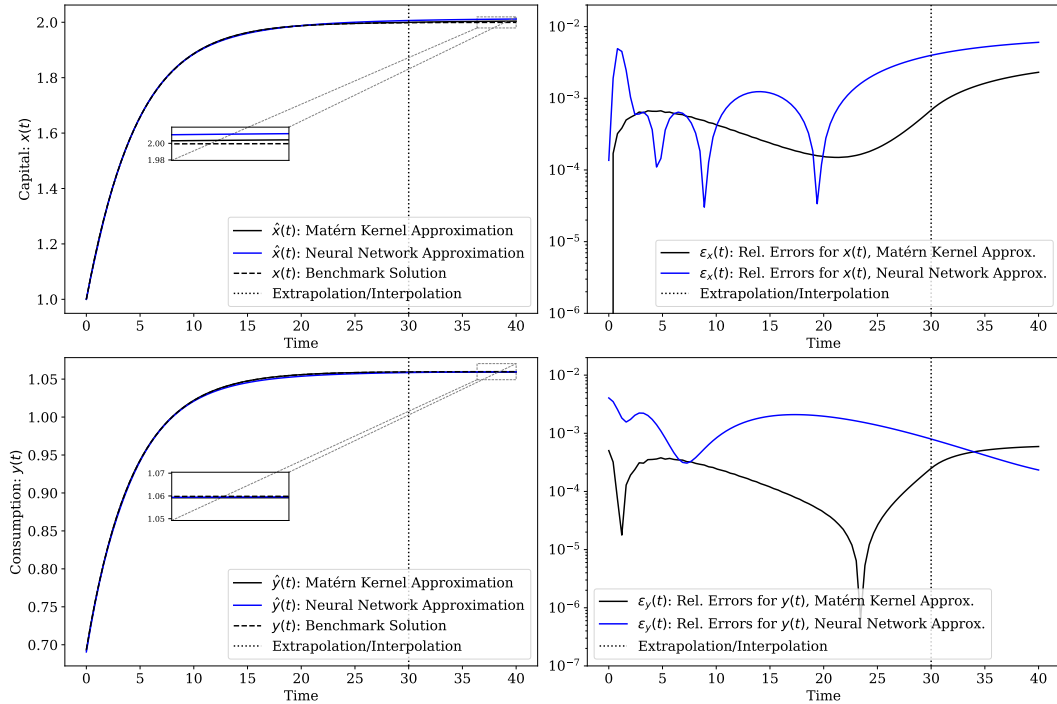


Figure 2: Neoclassical growth model (Eqs. (13) and (14)) solved without imposing the transversality condition (Eq. (15)). The top panels show the results for capital, $x(t)$, and the bottom panels show the results for consumption, $y(t)$. The left panels show the kernel machine and neural network approximations relative to the benchmark. The right panels display the absolute errors relative to the benchmark on a test set of 100 points from $t = 0$ to $t = 40$. In all cases, the ML methods recover the benchmark and even extrapolate well beyond the training data, despite solving an indeterminate problem and not directly calculating the steady state.

Results. Fig. 2 shows the results for both experiments.¹² Both the kernel interpolator and the neural network recover the unique equilibrium of economic interest almost perfectly, fulfilling Eq. (15) despite not being provided the steady-state as a boundary condition.

¹²The neural network maps t to $[x(t) \ y(t)]$. We use 4 hidden layers with 128 nodes and the Tanh activation function. In the final layer, the Softplus is used to ensure positive values for consumption and capital. For optimization, we use Adam with a learning rate of 10^{-3} . For the weights in Eq. (5) we use $\eta_1 = 0.4, \eta_2 = 0.4, \eta_4 = 0.2$.

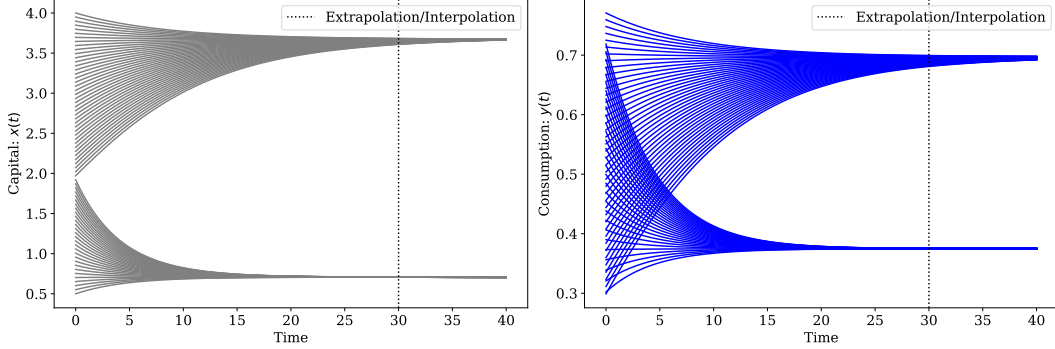


Figure 3: Neoclassical growth model (Eqs. (13) and (14)) with multiple steady states due to the concave-convex production function in Sec. 4.3. The left panel shows the solution trajectories for capital, $x(t)$, using Matérn Kernels for 70 different initial conditions $x_0 \in [0.5, 4]$. The right panel shows the solution trajectories for consumption, $y(t)$, for the same initial conditions. In all cases the ML method gives the correct trajectory for a given initial condition, despite not directly calculating the steady states. Furthermore, the left panel shows that the method is effective at learning the basins of attraction for the different steady states.

Robustness. While Theorem 1 demonstrates consistency, it is helpful to check our methods’ sensitivity to hyperparameters and features of \mathcal{D} : Appx. C.1 shows that our methods perform well with a much sparser set of time points; Appx. C.2 indicates low sensitivity to different kernel hyperparameters; and Appx. C.3 demonstrates that the approximation remains effective in the short- to medium-term even if \mathcal{D} does not approach the steady state.

4.3 Neoclassical Growth Model with Multiple Steady-States

We now turn to a more complex version of the neoclassical growth model (Eqs. (13) to (15)) where $f(x) := A \max\{x^a, b_1 x^a - b_2\}$, as in [42].¹³ This problem is still well-posed (as long as Eq. (15) is included) and hence has a unique trajectory for a given initial condition—which would lead towards one of the two steady states. This provides a significant challenge for classical algorithms, such as shooting methods, which rely on finding the steady state and using it as a finite-horizon boundary condition. All steady states need to be calculated, and the space of initial conditions must be sharply partitioned into different domains of attraction to know which steady state to use as the boundary condition for a particular initial condition.

Results. Fig. 3 shows the results using Matérn kernels for 70 different initial conditions across the basins of attraction for the two steady states. While the error relative to the benchmark solution is not shown, it is of comparable magnitude to that in Fig. 2.

It is worth noting that the kernel regression solutions find the “correct” steady state; i.e. the steady state that correctly corresponds with the supplied initial condition x_0 . Intuitively, this behavior is a consequence of the minimum Sobolev seminorm inductive bias. Consider the two possible trajectories x_0 to each of the two steady states: the trajectory with smaller gradients and less steep dynamics will have a smaller norm. In contrast, classical methods—which do not have a minimum norm inductive bias—require a mapping between initial conditions and the correct steady states.

4.4 Other Examples

In Appx. C.4 we examine a variation of the DAE formulation of the neoclassical growth problem of Sec. 4.2; i.e. a dynamical system where the $z(t)$ static variables are not eliminated. In addition, we test our methods on a standard model of human capital and economic growth (see Appx. D.1) as well as a model of optimal advertising used in the marketing literature [40] (see Appx. D.2).

¹³This function has a kink in $f'(x)$ at $\bar{x} = \left(\frac{b_2}{b_1 - 1}\right)^{\frac{1}{a}}$. Our baseline parameters are $A = 0.5, b_1 = 3.0, b_2 = 2.5, k_0 = 1.0, \delta = 0.1, r = 0.11$.

5 Related Work

Alternative methods for linearized systems. Perturbation solutions to models of economic dynamics use classic stability analysis of linear quadratic (LQ) control to find solutions that fulfill asymptotic boundary conditions (e.g., [7]). These methods use the linearity of time-invariant policies in LQ control and enforce stability by spectral methods (i.e., remove explosive roots that violate Eq. (4) by solving Riccati Equations). Our paper takes inspiration from this broader approach: algorithms which select non-explosive roots will be on the solution manifold and automatically fulfill Eq. (4).

ML for optimal control and economic dynamical systems. Recent literature on optimal control and robotics explores how to achieve stable solutions with deep neural networks [11, 12, 33, 34]. More directly within the economics literature, [18] discusses the intuitive connection between the inductive bias of deep neural networks and turnpikes [31] in dynamic economics, but does not provide theory. Our paper contributes to this literature, providing a formal argument on why the inductive bias of ML algorithms promotes stability in infinite-horizon control.

6 Discussion

While the class of problems in Sec. 2 focused on deterministic, continuous-time dynamical systems, these challenges exist in all dynamic models with forward-looking behavior or optimal control. Many questions in this research agenda remain:

- **How to model inequality and complementarity constraints?** Can Secs. 2 and 3 be extended to include inequality constraints (e.g., an additional primitive $C(\mathbf{x}(t), \mathbf{y}(t), \mathbf{z}(t)) \geq \mathbf{0}$)? This extension would allow us to incorporate a larger class of important models (e.g., lifecycle models of consumption, macroeconomic models of financial frictions, and Stackelberg games).
- **What is the role of inductive bias of ML algorithms for state-space representations and stochastic models?** In Sec. 2, we characterized deterministic, infinite-horizon models written in a sequence space, but many dynamic economic models are stochastic and more naturally written in a recursive, state-space representation. Does the inductive bias of ML algorithms applied to state-space formulations (e.g., approximating policy or value functions of the state) fulfill Eq. (4)?¹⁴
- **When are kernel methods and neural networks preferable to classic algorithms?** Beyond its purpose in formalizing the analysis, we have shown that kernel methods are fast and robust in practice, even in low dimensions. Classic algorithms such as shooting methods will likely dominate kernels when carefully tuned and where steady states are easy to solve, but ML methods might be directly useful in this problem domain.

References

- [1] D. Acemoglu. *Introduction to modern economic growth*. Princeton university press, 2008.
- [2] M. Azinovic and J. Žemlička. Economics-inspired neural networks with stabilizing homotopies. *arXiv preprint arXiv:2303.14802*, 2023.
- [3] M. Azinovic, L. Gaegauf, and S. Scheidegger. Deep equilibrium nets. *International Economic Review*, n/a(n/a), 2022. doi: <https://doi.org/10.1111/iere.12575>. URL <https://onlinelibrary.wiley.com/doi/abs/10.1111/iere.12575>.
- [4] M. Barnett, W. Brock, L. P. Hansen, R. Hu, and J. Huang. A deep learning analysis of climate change, innovation, and uncertainty, 2023.
- [5] M. Belkin. Fit without fear: remarkable mathematical phenomena of deep learning through the prism of interpolation. *Acta Numerica*, 30:203–248, 2021.

¹⁴Transversality conditions remain necessary conditions for problems to be well-posed in state-space representations of dynamic models. Even verifying them is difficult in practice because they must hold at every point in the state space and are written as expected discounted values of random trajectories. For more details, see [28] and [19].

- [6] L. Benveniste and J. Scheinkman. Duality theory for dynamic optimization models of economics: The continuous time case. *Journal of Economic Theory*, 27(1):1–19, 1982. ISSN 0022-0531. doi: [https://doi.org/10.1016/0022-0531\(82\)90012-6](https://doi.org/10.1016/0022-0531(82)90012-6). URL <https://www.sciencedirect.com/science/article/pii/0022053182900126>.
- [7] O. J. Blanchard and C. M. Kahn. The solution of linear difference models under rational expectations. *Econometrica: Journal of the Econometric Society*, pages 1305–1311, 1980.
- [8] O. J. Blanchard and M. W. Watson. Bubbles, rational expectations and financial markets, 1982.
- [9] H. Brezis and H. Brézis. *Functional analysis, Sobolev spaces and partial differential equations*, volume 2. Springer, 2011.
- [10] B. Calderhead, M. Girolami, and N. Lawrence. Accelerating Bayesian inference over nonlinear differential equations with Gaussian processes. *Advances in neural information processing systems*, 21, 2008.
- [11] Y.-C. Chang, N. Roohi, and S. Gao. Neural lyapunov control. In H. Wallach, H. Larochelle, A. Beygelzimer, F. d'Alché-Buc, E. Fox, and R. Garnett, editors, *Advances in Neural Information Processing Systems*, volume 32. Curran Associates, Inc., 2019. URL https://proceedings.neurips.cc/paper_files/paper/2019/file/2647c1dba23bc0e0f9cdf75339e120d2-Paper.pdf.
- [12] G. Chen. Deep neural network approximations for the stable manifolds of the hamilton-jacobi equations, 2023.
- [13] R. T. Chen, Y. Rubanova, J. Bettencourt, and D. K. Duvenaud. Neural ordinary differential equations. *Advances in neural information processing systems*, 31, 2018.
- [14] G. Chichilnisky. Nonlinear functional analysis and optimal economic growth. *Journal of Mathematical Analysis and Applications*, 61(2):504–520, 1977. ISSN 0022-247X. doi: [https://doi.org/10.1016/0022-247X\(77\)90134-2](https://doi.org/10.1016/0022-247X(77)90134-2). URL <https://www.sciencedirect.com/science/article/pii/0022247X77901342>.
- [15] D. Childers, J. Fernández-Villaverde, J. Perla, C. Rackauckas, and P. Wu. Differentiable state space models and hamiltonian monte carlo estimation. *Working Paper*, 2022.
- [16] B. T. Diba and H. I. Grossman. The theory of rational bubbles in stock prices. *The Economic Journal*, 98(392):746–754, 1988. ISSN 00130133, 14680297. URL <http://www.jstor.org/stable/2233912>.
- [17] M. Ebrahimi Kahou, J. Fernández-Villaverde, J. Perla, and A. Sood. Exploiting symmetry in high-dimensional dynamic programming. Working Paper 28981, National Bureau of Economic Research, July 2021. URL <http://www.nber.org/papers/w28981>.
- [18] M. Ebrahimi Kahou, J. Fernández-Villaverde, S. Gomez, J. Perla, and J. Rosa. Spooky boundaries at a distance: Exploring transversality and stability with deep learning. *Working Paper*, 2024.
- [19] J. Fernández-Villaverde, J. F. Rubio-Ramírez, and F. Schorfheide. Solution and estimation methods for dsge models. In *Handbook of macroeconomics*, volume 2, pages 527–724. Elsevier, 2016.
- [20] J. Fernández-Villaverde, S. Hurtado, and G. Nuño. Financial frictions and the wealth distribution. *Econometrica*, 91(3):869–901, 2023. doi: <https://doi.org/10.3982/ECTA18180>. URL <https://onlinelibrary.wiley.com/doi/abs/10.3982/ECTA18180>.
- [21] J. Hadamard. Sur les problèmes aux dérivées partielles et leur signification physique. *Princeton university bulletin*, pages 49–52, 1902.
- [22] J. Hadamard and J. Hadamard. Le problème de cauchy et les équations aux dérivées partielles linéaires hyperboliques: leçons professées à l'université yale. 1932.
- [23] J. Han, A. Jentzen, and W. E. Solving high-dimensional partial differential equations using deep learning. *Proceedings of the National Academy of Sciences*, 115(34):8505–8510, Aug. 2018. ISSN 1091-6490. doi: 10.1073/pnas.1718942115. URL <http://dx.doi.org/10.1073/pnas.1718942115>.
- [24] J. Han, Y. Yang, and W. E. Deepham: A global solution method for heterogeneous agent models with aggregate shocks, 2022.
- [25] W. Jungerman. Dynamic monopsony and human capital. Working Paper, 2023.
- [26] H. Kase, L. Melosi, and M. Rottner. *Estimating nonlinear heterogeneous agents models with neural networks*. Centre for Economic Policy Research, 2022.

- [27] N. Kovachki, Z. Li, B. Liu, K. Azizzadenesheli, K. Bhattacharya, A. Stuart, and A. Anandkumar. Neural operator: Learning maps between function spaces with applications to pdes. *Journal of Machine Learning Research*, 24(89):1–97, 2023.
- [28] L. Ljungqvist and T. Sargent. *Recursive Macroeconomic Theory, fourth edition*. MIT Press, 2018. ISBN 9780262038669. URL <https://books.google.ca/books?id=IG1qDwAAQBAJ>.
- [29] C. Ma and L. Ying. On linear stability of sgd and input-smoothness of neural networks. *Advances in Neural Information Processing Systems*, 34:16805–16817, 2021.
- [30] L. Maliar, S. Maliar, and P. Winant. Deep learning for solving dynamic economic models. *Journal of Monetary Economics*, 122:76–101, 2021. ISSN 0304-3932. doi: <https://doi.org/10.1016/j.jmoneco.2021.07.004>. URL <https://www.sciencedirect.com/science/article/pii/S0304393221000799>.
- [31] L. W. McKenzie. Turnpike theory. *Econometrica*, 44(5):841–865, 1976. ISSN 00129682, 14680262. URL <http://www.jstor.org/stable/1911532>.
- [32] P. Michel. On the transversality condition in infinite horizon optimal problems. *Econometrica: Journal of the Econometric Society*, pages 975–985, 1982.
- [33] T. Nakamura-Zimmerer, Q. Gong, and W. Kang. Neural network optimal feedback control with guaranteed local stability. *IEEE Open Journal of Control Systems*, 1:210–222, 2022. doi: 10.1109/OJCSYS.2022.3205863.
- [34] T. Nakamura-Zimmerer, Q. Gong, and W. Kang. Neural network optimal feedback control with enhanced closed loop stability. In *2022 American Control Conference (ACC)*, pages 2373–2378. IEEE, 2022.
- [35] E. Pardoux and S. Tang. Forward-backward stochastic differential equations and quasilinear parabolic pdes. *Probability theory and related fields*, 114:123–150, 1999.
- [36] J. Payne, A. Revei, and Y. Yang. Deep learning for search and matching models, 2024. URL <https://dx.doi.org/10.2139/ssrn.4768566>.
- [37] C. E. Rasmussen and C. Williams. *Gaussian processes for machine learning*, volume 1. MIT Press, 2006.
- [38] S. Scheidegger and I. Bilonis. Machine learning for high-dimensional dynamic stochastic economies. *Journal of Computational Science*, 33:68–82, 2019. ISSN 1877-7503. doi: <https://doi.org/10.1016/j.jocs.2019.03.004>. URL <https://www.sciencedirect.com/science/article/pii/S1877750318306161>.
- [39] M. Schober, D. K. Duvenaud, and P. Hennig. Probabilistic ode solvers with runge-kutta means. *Advances in neural information processing systems*, 27, 2014.
- [40] S. P. Sethi. Optimal control of the vidale-wolfe advertising model. *Operations research*, 21(4):998–1013, 1973.
- [41] J. Sirignano and K. Spiliopoulos. Dgm: A deep learning algorithm for solving partial differential equations. *Journal of Computational Physics*, 375:1339–1364, Dec. 2018. ISSN 0021-9991. doi: 10.1016/j.jcp.2018.08.029. URL <http://dx.doi.org/10.1016/j.jcp.2018.08.029>.
- [42] A. K. Skiba. Optimal growth with a convex-concave production function. *Econometrica*, 46:527–539, 1978. ISSN 00129682, 14680262. URL <http://www.jstor.org/stable/1914229>.
- [43] A. N. Tikhonov. On the solution of ill-posed problems and the method of regularization. In *Doklady akademii nauk*, volume 151, pages 501–504. Russian Academy of Sciences, 1963.
- [44] C. L. Van, R. Boucekkine, and C. Saglam. Optimal control in infinite horizon problems: a sobolev space approach. *Economic Theory*, 32(3):497–509, 2007.
- [45] M. L. Vidale and H. Wolfe. An operations-research study of sales response to advertising. *Operations research*, 5(3):370–381, 1957.
- [46] M. J. Wainwright. *High-dimensional statistics: A non-asymptotic viewpoint*, volume 48. Cambridge university press, 2019.
- [47] T. A. Weber. An infinite-horizon maximum principle with bounds on the adjoint variable. *Journal of Economic Dynamics and Control*, 30(2):229–241, 2006.
- [48] H. Wendland. Scattered data approximation. 2004.
- [49] R. A. Willoughby. Solutions of ill-posed problems (a. n. tikhonov and v. y. arsenin). *SIAM Review*, 21(2): 266–267, 1979. doi: 10.1137/1021044. URL <https://doi.org/10.1137/1021044>.

A Connection Between Sobolev- $P, 2$ Spaces and Matérn RKHS

Let $k_{\nu,\ell}(\cdot, \cdot) : \mathbb{R} \times \mathbb{R} \rightarrow \mathbb{R}$ denote the Matérn covariance function with smoothness ν and lengthscale ℓ . For the purposes of this paper, we will define $k_{\nu,\ell}$ as:

$$k_{\nu,\ell}(t, t') = \kappa(|t - t'|), \quad \widehat{\kappa}(\omega) := (1 + \ell^2 \omega^2)^{-\nu-1/2}, \quad (16)$$

where $\widehat{(\cdot)}$ corresponds to the Fourier transform. Note that Eq. (16) corresponds to the standard Matérn kernel definition [37] after appropriately scaling the inputs and outputs. $\nabla^{(r)} k_{\nu,\ell}(\cdot, \cdot)$ will denote the r^{th} derivative of $k_{\nu,\ell}$ with respect to its first argument.

Given some interval $[0, T] \subseteq \mathbb{R}$, $\mathcal{H}^{\nu,\ell}([0, T])$ denotes the RKHS of $[0, T] \rightarrow \mathbb{R}$ functions where the reproducing kernel is equal to $k_{\nu,\ell}$. $\mathcal{W}^{P,2}([0, T])$ denotes the Sobolev- $P, 2$ space of $[0, T] \rightarrow \mathbb{R}$ functions. Whenever possible we will drop the superscripts for $\mathcal{H}^{\nu,\ell}([0, T])$.

Proposition 1 (Equivalence of $\mathcal{W}^{P,2}$ and $\mathcal{H}^{\nu,\ell}$). *For any positive integer P , any $\ell > 0$, and any $\nu = P - 1/2$ there exists positive constants $C_1(\nu, \ell)$ and $C_2(\nu, \ell)$ so that*

$$C_1(\nu, \ell) \|w\|_{\mathcal{W}^{P,2}([0, T])} \leq \|w\|_{\mathcal{H}^{\nu,\ell}([0, T])} \leq C_2(\nu, \ell) \|w\|_{\mathcal{W}^{P,2}([0, T])}.$$

for all $w \in \mathcal{W}^{P,2}$. In other words, the Sobolev norm $\|\cdot\|_{\mathcal{W}^{P,2}([0, T])}$ and the RKHS norm $\|\cdot\|_{\mathcal{H}^{\nu,\ell}([0, T])}$ are equivalent, and thus $\mathcal{W}^{P,2}([0, T]) = \mathcal{H}^{\nu,\ell}([0, T])$.

Proof. We begin by first establishing an equivalence between $\mathcal{W}^{P,2}(\mathbb{R})$ and $\mathcal{H}^{\ell,\nu}(\mathbb{R})$. In the Fourier domain, the Sobolev norm for $\mathbb{R} \rightarrow \mathbb{R}$ functions is given by

$$\|w\|_{\mathcal{W}^{P,2}(\mathbb{R})} = \left\| \widehat{w}(\cdot) (1 + (\cdot)^2)^{P/2} \right\|_{L_2(\mathbb{R})},$$

and, for any RKHS $\mathcal{H}(\mathbb{R})$ with stationary reproducing kernels, the RKHS norm for $\mathbb{R} \rightarrow \mathbb{R}$ functions is given by

$$\|w\|_{\mathcal{H}(\mathbb{R})} = \left\| \widehat{w}(\cdot) (\widehat{\kappa}(\cdot))^{-1/2} \right\|_{L_2(\mathbb{R})}$$

The Matérn kernel, as defined in Eq. (16), has a Fourier transform that decays at a rate of $(1 + |\cdot|^2)^{-P}$ and thus $\|\cdot\|_{\mathcal{H}^{\nu,\ell}(\mathbb{R})}$ is bounded above and below by a constant multiple of $\|\cdot\|_{\mathcal{W}^{P,2}(\mathbb{R})}$ where the constant only depends on ℓ . This argument can be generalized to prove an equivalence between $\mathcal{W}^{P,2}([0, T])$ and $\mathcal{H}^{\ell,\nu}([0, T])$, as the domain $[0, T]$ trivially has a Lipschitz boundary. (See [48, Corollary 10.48] for details.) \square

Corollary 1.1 (Equality of $\mathcal{W}^{P,2}$ and $\mathcal{H}^{\nu,\ell}$ with specific ν, ℓ values). *For any P , there exists a value of ℓ so that, for all $w \in \mathcal{W}^{P,2}([0, T])$:*

$$\|w\|_{\mathcal{W}^{P,2}([0, T])} = \|w\|_{\mathcal{H}^{P-1/2,\ell}([0, T])}.$$

B Proof of Theorem 1

Theorem 1 (Restated). *Given some $0 < K < \infty$, let \mathbb{S} be the set of functions $(\mathbf{x}, \mathbf{y}, \mathbf{z})$ that satisfy Eqs. (1) to (3) with $\mathbf{x}(0) = \mathbf{x}_0$ and $\|\mathbf{y}(0)\|_\infty, \|\mathbf{z}(0)\|_\infty \leq K$. If*

- $t \in \mathcal{D}$ are drawn uniformly i.i.d. from $[0, T]$;
- \mathbf{F} , \mathbf{G} , and \mathbf{H} in Eqs. (1) to (3) are Lipschitz with respect to $\|\cdot\|_\infty$; and
- \mathbf{F} and \mathbf{G} have Lipschitz first derivatives and \mathbf{H} has Lipschitz first and second derivatives,

then then the solutions $\hat{\mathbf{x}}_N, \hat{\mathbf{y}}_N, \hat{\mathbf{z}}_N$ from Eq. (7) with the Matern-1/2 kernel satisfies Eqs. (1) to (3) almost everywhere in the limit as $N \rightarrow \infty$ and

$$\lim_{N \rightarrow \infty} \sum_{m=1}^{M_x} |\hat{\mathbf{x}}_N^{(m)}|_{\mathcal{W}^{2,2}([0, T])}^2 + \sum_{m=1}^{M_y} |\hat{\mathbf{y}}_N^{(m)}|_{\mathcal{W}^{2,2}([0, T])}^2 + \sum_{m=1}^{M_z} |\hat{\mathbf{z}}_N^{(m)}|_{\mathcal{W}^{2,2}([0, T])}^2 \\ \stackrel{\text{a.s.}}{=} \inf_{(\mathbf{x}, \mathbf{y}, \mathbf{z}) \in \mathbb{S}} \sum_{m=1}^{M_x} |\hat{\mathbf{x}}^{(m)}|_{\mathcal{W}^{2,2}([0, T])}^2 + \sum_{m=1}^{M_y} |\hat{\mathbf{y}}^{(m)}|_{\mathcal{W}^{2,2}([0, T])}^2 + \sum_{m=1}^{M_z} |\hat{\mathbf{z}}^{(m)}|_{\mathcal{W}^{2,2}([0, T])}^2.$$

Throughout this proof we will drop the domain $[0, T]$ from the \mathcal{W} and \mathcal{H} notation for brevity. We break up this proof into a series of lemmas.

Lemma 1. *For every $(\mathbf{x}, \mathbf{y}, \mathbf{z}) \in \mathbb{S}$, the functions $x^{(1)}, \dots, x^{(M_x)}$, $y^{(1)}, \dots, y^{(M_y)}$, and $z^{(1)}, \dots, z^{(M_z)}$, are all elements of $\mathcal{W}^{P+1,2}$.*

Proof. By Lipschitz continuity of \mathbf{F} , \mathbf{G} , \mathbf{H} and the Cauchy-Lipschitz-Picard theorem [e.g. 9, Thm. 7.3], we have that every $(\mathbf{x}, \mathbf{y}, \mathbf{z}) \in \mathbb{S}$ are continuous and continuously differentiable over $[0, \infty)$. This fact implies that $\mathbf{x}, \mathbf{y}, \mathbf{z}$ and $\dot{\mathbf{x}}, \dot{\mathbf{y}}, \dot{\mathbf{z}}$ are bounded over $[0, T]$. Assuming that $\dot{\mathbf{x}}, \dots, \dot{\mathbf{x}}^{(k)}$, $\dot{\mathbf{y}}, \dots, \dot{\mathbf{y}}^{(k)}$, $\dot{\mathbf{z}}, \dots, \dot{\mathbf{z}}^{(k)}$ are also bounded, consider $\mathbf{x}^{(k+1)}, \mathbf{y}^{(k+1)}, \mathbf{z}^{(k+1)}$ for $k \leq P$:

$$\begin{aligned} \mathbf{x}^{(k+1)}(t) &= \mathbf{F}^{(k)}(\mathbf{x}(t), \mathbf{y}(t), \mathbf{z}(t)) \\ \mathbf{y}^{(k+1)}(t) &= \mathbf{G}^{(k)}(\mathbf{x}(t), \mathbf{y}(t), \mathbf{z}(t)) \\ \mathbf{0} &= \mathbf{H}^{(k)}(\mathbf{x}(t), \mathbf{y}(t), \mathbf{z}(t)) \end{aligned}$$

By Faà di Bruno's formula, $\mathbf{F}^{(k)}(\mathbf{x}(t), \mathbf{y}(t), \mathbf{z}(t))$ is a polynomial involving the terms

- $\mathbf{F}(\mathbf{x}(t), \mathbf{y}(t), \mathbf{z}(t)), \dots, \mathbf{F}^{(k+1)}(\mathbf{x}(t), \mathbf{y}(t), \mathbf{z}(t))$,
- $\mathbf{x}(t), \dots, \mathbf{x}^{(k-1)}(t)$,
- $\mathbf{y}(t), \dots, \mathbf{y}^{(k-1)}(t)$, and
- $\mathbf{z}(t), \dots, \mathbf{z}^{(k-1)}(t)$.

By inductive assumption, the latter terms are bounded over $[0, T]$. Moreover, the range of $\mathbf{x}(t)$, $\mathbf{y}(t)$, and $\mathbf{z}(t)$ will be a compact interval, and thus $\mathbf{F}(\mathbf{x}(t), \mathbf{y}(t), \mathbf{z}(t)), \dots, \mathbf{F}^{(k+1)}(\mathbf{x}(t), \mathbf{y}(t), \mathbf{z}(t))$, will be bounded by Lipschitz continuity. Therefore, $\mathbf{x}, \dots, \mathbf{x}^{(P+1)}$ are all bounded over $[0, T]$. Analogous results hold for $\mathbf{y}, \dots, \mathbf{y}^{(P+1)}$ and $\mathbf{z}, \dots, \mathbf{z}^{(P+1)}$. Since bounded functions are trivially square integrable, we have that

- $\|x^{(1)}\|_{\mathcal{W}^{P+1,2}}, \dots, \|x^{(M_x)}\|_{\mathcal{W}^{P+1,2}} < \infty$,
- $\|y^{(1)}\|_{\mathcal{W}^{P+1,2}}, \dots, \|y^{(M_y)}\|_{\mathcal{W}^{P+1,2}} < \infty$, and
- $\|z^{(1)}\|_{\mathcal{W}^{P+1,2}}, \dots, \|z^{(M_z)}\|_{\mathcal{W}^{P+1,2}} < \infty$.

□

Lemma 2. *Define $M = M_x + M_y + M_z$, and define $\mathcal{W}_M^{P+1,2}$ as the vector-valued reproducing kernel Hilbert space of functions $(\mathbf{x}(\cdot), \mathbf{y}(\cdot), \mathbf{z}(\cdot)) : [0, T] \rightarrow \mathbb{R}^M$ with the property that*

$$\mathbf{w} \in \mathcal{W}_M^{P+1,2} \Leftrightarrow w^{(m)} \in \mathcal{W}^{P+1,2} \quad \forall m \in [1, M]$$

Then the set \mathbb{S} is closed with respect to $\|\cdot\|_{\mathcal{W}_M^{P+1,2}}$.

Proof. By standard theory of vector-valued reproducing kernel Hilbert spaces, the norm associated with $\mathcal{W}_M^{P+1,2}$ is

$$\|(\mathbf{x}, \mathbf{y}, \mathbf{z})\|_{\mathcal{W}_M^{P+1,2}} := \sqrt{\sum_{m=1}^{M_x} \|\hat{x}_N^{(m)}\|_{\mathcal{W}^{P+1,2}}^2 + \sum_{m=1}^{M_y} \|\hat{y}_N^{(m)}\|_{\mathcal{W}^{P+1,2}}^2 + \sum_{m=1}^{M_z} \|\hat{z}_N^{(m)}\|_{\mathcal{W}^{P+1,2}}^2}$$

Consider a Cauchy sequence $(\mathbf{x}_n, \mathbf{y}_n, \mathbf{z}_n) \in \mathbb{S}$ w.r.t. $\|\cdot\|_{\mathcal{W}_M^{P+1,2}}$. By Lemma 1, we have that $x_n^{(m)} \in \mathcal{W}^{P+1,2}$ for all $m \in [1, M_x]$. By completeness of $\mathcal{W}^{P+1,2}$, we have that $x_n^{(m)} \rightarrow x^{(m)}$ for some $x^{(m)} \in \mathcal{W}^{P+1,2}$; i.e. for every ϵ , there exists some n' such that $\|y_{n'}^{(m)} - y^{(m)}\|_{\mathcal{W}^{P+1,2}} < \epsilon$.

$$\begin{aligned} \sup_{t \in [0, T]} \|x_{n'}^{(m)}(t) - x^{(m)}(t)\|_\infty &= \sup_{t \in [0, T]} \left\langle k(t, \cdot), x_{n'}^{(m)}(t) - x^{(m)}(t) \right\rangle_{\mathcal{W}^{P+1,2}} \\ &\leq \sup_{t \in [0, T]} \|k(t, \cdot)\|_{\mathcal{W}^{P+1,2}} \|x_{n'}^{(m)}(t) - x^{(m)}(t)\|_{\mathcal{W}^{P+1,2}} \\ &\leq C \|x_{n'}^{(m)}(t) - x^{(m)}(t)\|_{\mathcal{W}^{P+1,2}} < C\epsilon, \end{aligned}$$

where $k(\cdot, \cdot)$ is the reproducing kernel associated with $\mathcal{W}^{P+1,2}$ and C is some universal constant. The penultimate inequality comes from fact that $\mathcal{W}^{P+1,2}$ is equivalent to a Matérn RKHS which has a bounded-everywhere reproducing kernel. Thus, $x_{n'}^{(m)}$ converges uniformly to $x^{(m)}$, and so

$$\begin{aligned} \dot{\mathbf{x}}(t) &= \lim_{n \rightarrow \infty} \dot{\mathbf{x}}_n(t) = \lim_{n \rightarrow \infty} \mathbf{F}(\mathbf{x}_n(t), \mathbf{y}_n(t), \mathbf{z}_n(t)) \\ &= \mathbf{F}(\lim_{n \rightarrow \infty} \mathbf{x}_n(t), \lim_{n \rightarrow \infty} \mathbf{y}_n(t), \lim_{n \rightarrow \infty} \mathbf{z}_n(t)) = \mathbf{F}(\mathbf{x}(t), \mathbf{y}(t), \mathbf{z}(t)) \end{aligned}$$

where the penultimate equality comes from the continuity of \mathbf{F} . Analogous results hold for \mathbf{y}_n and \mathbf{z}_n . Moreover, by uniform convergence we have that $\|\mathbf{y}(0) - \mathbf{y}_n(0)\|_\infty$ and $\|\mathbf{z}(0) - \mathbf{z}_n(0)\|_\infty$ are arbitrarily small and thus $\|\mathbf{y}(0)\|_\infty, \|\mathbf{z}(0)\|_\infty < K$. Therefore $(\mathbf{x}, \mathbf{y}, \mathbf{z}) \in \mathbb{S}$. \square

Lemma 3. Denote M and $\mathcal{W}_M^{P+1,2}$ as in Lemma 2. Let

$$\begin{aligned} B &:= \inf_{(\mathbf{x}, \mathbf{y}, \mathbf{z}) \in \mathbb{S}} \sum_{m=1}^{M_x} |x_N^{(m)}|_{\mathcal{W}^{P+1,2}}^2 + \sum_{m=1}^{M_y} |y_N^{(m)}|_{\mathcal{W}^{P+1,2}}^2 + \sum_{m=1}^{M_z} |z_N^{(m)}|_{\mathcal{W}^{P+1,2}}^2 \\ &= \inf_{(\mathbf{x}, \mathbf{y}, \mathbf{z}) \in \mathbb{S}} \sum_{m=1}^{M_x} \|\dot{x}_N^{(m)}\|_{\mathcal{W}^{P,2}}^2 + \sum_{m=1}^{M_y} \|\dot{y}_N^{(m)}\|_{\mathcal{W}^{P,2}}^2 + \sum_{m=1}^{M_z} \|\dot{z}_N^{(m)}\|_{\mathcal{W}^{P,2}}^2 \\ &= \inf_{(\mathbf{x}, \mathbf{y}, \mathbf{z}) \in \mathbb{S}} \|(\dot{\mathbf{x}}, \dot{\mathbf{y}}, \dot{\mathbf{z}})\|_{\mathcal{W}_M^{P,2}} \end{aligned}$$

Then there exists some $(\mathbf{x}^*, \mathbf{y}^*, \mathbf{z}^*) \in \mathbb{S}$ that achieves this infimum.

Proof. Define the operator $D : \mathcal{W}_M^{P+1,2} \rightarrow \mathcal{W}_M^{P+1,2}$ as $D(\mathbf{x}, \mathbf{y}, \mathbf{z}) = (\dot{\mathbf{x}}, \dot{\mathbf{y}}, \dot{\mathbf{z}})$, where here $\dot{\mathbf{x}}, \dot{\mathbf{y}}, \dot{\mathbf{z}}$ denote weak derivatives. Note that D is a surjective and bounded linear operator between two Hilbert spaces:

$$\begin{aligned} \|(\mathbf{x}, \mathbf{y}, \mathbf{z})\|_{\mathcal{W}_M^{P+1,2}}^2 &= \sum_{m=1}^{M_x} \|\hat{x}_N^{(m)}\|_{\mathcal{W}^{P+1,2}}^2 + \sum_{m=1}^{M_y} \|\hat{y}_N^{(m)}\|_{\mathcal{W}^{P+1,2}}^2 + \sum_{m=1}^{M_z} \|\hat{z}_N^{(m)}\|_{\mathcal{W}^{P+1,2}}^2 \\ &= \sum_{m=1}^{M_x} \|\dot{x}_N^{(m)}\|_{\mathcal{W}^{P,2}}^2 + \sum_{m=1}^{M_y} \|\dot{y}_N^{(m)}\|_{\mathcal{W}^{P,2}}^2 + \sum_{m=1}^{M_z} \|\dot{z}_N^{(m)}\|_{\mathcal{W}^{P,2}}^2 \\ &= \|(\dot{\mathbf{x}}, \dot{\mathbf{y}}, \dot{\mathbf{z}})\|_{\mathcal{W}_M^{P,2}}^2 \end{aligned}$$

Furthermore, note that the nullspace of D (i.e. the set of constant functions) is a closed set. Therefore, since $\mathbb{S} \subset \mathcal{W}_M^{P+1,2}$ is a closed subset of a Hilbert space (Lemma 2), $\dot{\mathbb{S}} := D(\mathbb{S}) \subset \mathcal{W}_M^{P+1,2}$ is also closed subset of a Hilbert space [see e.g. 9, Exercise 2.10]. By the existence portion of the Hilbert projection theorem, there exists a (potentially non-unique) minimum $\mathcal{W}_M^{P,2}$ -norm element of $\dot{\mathbb{S}}$ (i.e. there exists some $(\dot{\mathbf{x}}^*, \dot{\mathbf{y}}^*, \dot{\mathbf{z}}^*) \in \dot{\mathbb{S}}$ such that $\|(\dot{\mathbf{x}}^*, \dot{\mathbf{y}}^*, \dot{\mathbf{z}}^*)\|_{\mathcal{W}_M^{P,2}} = \inf_{(\mathbf{x}, \mathbf{y}, \mathbf{z}) \in \mathbb{S}} \|(\dot{\mathbf{x}}, \dot{\mathbf{y}}, \dot{\mathbf{z}})\|_{\mathcal{W}_M^{P,2}}$. We conclude the proof by setting $(\mathbf{x}^*, \mathbf{y}^*, \mathbf{z}^*)$ to be some element in \mathbb{S} such that $(\dot{\mathbf{x}}^*, \dot{\mathbf{y}}^*, \dot{\mathbf{z}}^*) = D(\mathbf{x}^*, \mathbf{y}^*, \mathbf{z}^*)$. \square

Lemma 4. For any $0 < C < \infty$, define the sets

$$\begin{aligned} \mathbb{F}^C &:= \{w \in \mathcal{W}^{P,2} : \|w\|_{\mathcal{W}^{P,2}} \leq C\} \\ \int \mathbb{F}^C &:= \left\{ \int_0^{\cdot} w(\tau) d\tau : w \in \mathbb{F}^C \right\}. \end{aligned}$$

Denoting $\widehat{\mathcal{R}}_N$ as the empirical Rademacher complexity for some dataset $t_1, \dots, t_N \in [0, T]$, we have that

$$\widehat{\mathcal{R}}_N(\mathbb{F}^C) \lesssim CN^{-1/2}, \quad \widehat{\mathcal{R}}_N(\int \mathbb{F}^C) \lesssim TCN^{-1/2}.$$

Proof. The Rademacher complexity $\widehat{\mathcal{R}}_N(\mathbb{F}^C) \lesssim CN^{-1/2}$ follows a standard result for reproducing kernel Hilbert spaces, using the fact that $\mathcal{W}^{P,2}$ is equivalent to the Matérn RKHS which has a bounded-everywhere reproducing kernel. Bounding the Rademacher complexity of $\int \mathbb{F}^C$ mirrors the standard proof of the $\widehat{\mathcal{R}}_N(\mathbb{F}^C)$ bound:

$$\begin{aligned}
\widehat{\mathcal{R}}(\int \mathbb{F}^C) &:= \mathbb{E}_{\epsilon_i} \left[\sup_{w \in \mathcal{W}^{P,2}} \frac{1}{N} \sum_{i=1}^N \epsilon_i \int_0^{t_i} w(\tau) d\tau \right] && (\epsilon_i \stackrel{\text{i.i.d.}}{\sim} \text{Rad}) \\
&= \mathbb{E}_{\epsilon_i} \left[\sup_{w \in \mathcal{W}^{P,2}} \left\langle \frac{1}{N} \sum_{i=1}^N \epsilon_i \int_0^{t_i} k(\tau, \cdot) d\tau, w(\cdot) \right\rangle_{\mathcal{W}^{P,2}} \right] \\
&\leq \mathbb{E}_{\epsilon_i} \left[\left\| \frac{C}{N} \sum_{i=1}^N \epsilon_i \int_0^{t_i} k(\tau, \cdot) d\tau \right\|_{\mathcal{W}^{P,2}} \right] && (\text{Cauchy-Schwarz inequality}) \\
&\leq \sqrt{\mathbb{E}_{\epsilon_i} \left[\left\| \frac{C}{N} \sum_{i=1}^N \epsilon_i \int_0^{t_i} k(\tau, \cdot) d\tau \right\|_{\mathcal{W}^{P,2}}^2 \right]} && (\text{Jensen inequality}) \\
&= \sqrt{\mathbb{E}_{\epsilon_i} \left[\frac{C^2}{N^2} \sum_{i,j=1}^N \epsilon_i \epsilon_j \left\langle \int_0^{t_i} k(\tau, \cdot) d\tau, \int_0^{t_j} k(\tau, \cdot) d\tau \right\rangle_{\mathcal{W}^{P,2}} \right]} \\
&= \sqrt{\frac{C^2}{N^2} \sum_i \left\| \int_0^{t_i} k(\tau, \cdot) d\tau \right\|_{\mathcal{W}^{P,2}}^2} && (\epsilon_i \text{ are uncorrelated}) \\
&\leq \sqrt{\frac{C^2}{N^2} \sum_i \left(\int_0^{t_i} \|k(\tau, \cdot)\|_{\mathcal{W}^{P,2}} d\tau \right)^2} && (\text{triangle inequality}) \\
&\leq \sqrt{\frac{C^2}{N^2} \sum_i \left(\int_0^T \sup_{t \in [0, T]} \|k(t, \cdot)\|_{\mathcal{W}^{P,2}} d\tau \right)^2} \\
&= TCN^{-1/2} \sup_{t \in [0, T]} \|k(t, \cdot)\|_{\mathcal{W}^{P,2}}.
\end{aligned}$$

Recognizing that $k(t, \cdot)$ is equivalent to a bounded-everywhere reproducing kernel completes the proof. \square

Lemma 5. Define M and $\mathcal{W}_D^{P,2}$ as in Lemma 2. For any $0 < C < \infty$, define the sets

$$\begin{aligned}
\mathbb{F}_M^C &:= \left\{ (\dot{\mathbf{x}}, \dot{\mathbf{y}}, \dot{\mathbf{z}}) \in \mathcal{W}_M^{P,2} : \|(\dot{\mathbf{x}}, \dot{\mathbf{y}}, \dot{\mathbf{z}})\|_{\mathcal{W}_D^{P,2}} \leq C \right\} \\
\int \mathbb{F}_M^C &:= \left\{ \int_0^{(\cdot)} (\dot{\mathbf{x}}(\tau), \dot{\mathbf{y}}(\tau), \dot{\mathbf{z}}(\tau)) d\tau : (\dot{\mathbf{x}}, \dot{\mathbf{y}}, \dot{\mathbf{z}}) \in \mathbb{F} \right\}
\end{aligned}$$

Then $\widehat{\mathcal{R}}_N(\mathbb{F}_M^C) \lesssim CMN^{-1/2}$ and $\widehat{\mathcal{R}}_N(\int \mathbb{F}_M^C) \lesssim TMCN^{-1/2}$.

Proof. The proof follows a standard summation argument for Rademacher complexity:

$$\begin{aligned}
& \widehat{\mathcal{R}}(\mathbb{F}_M^C) \\
& := \mathbb{E} \left[\sup_{(\dot{\mathbf{x}}, \dot{\mathbf{y}}, \dot{\mathbf{z}}) \in \mathcal{W}_M^{P,2}} \frac{1}{N} \sum_{i=1}^N \left(\sum_{j_x=1}^{M_x} \epsilon_{ij_x} \dot{\mathbf{x}}^{(j_x)}(t_i) + \sum_{j_y=1}^{M_y} \epsilon_{ij_y} \dot{\mathbf{y}}^{(j_y)}(t_i) + \sum_{j_z=1}^{M_z} \epsilon_{ij_z} \dot{\mathbf{z}}^{(j_z)}(t_i) \right) \right] \\
& \qquad \qquad \qquad (\epsilon_{ij_x}, \epsilon_{ij_y}, \epsilon_{ij_z} \stackrel{\text{i.i.d.}}{\sim} \text{Rad}) \\
& \leq \sum_{j_x=1}^{M_x} \mathbb{E} \left[\sup_{\dot{\mathbf{x}}^{(j_x)} \in \mathcal{W}^{P,2}} \frac{1}{N} \sum_{i=1}^N \epsilon_{ij_x} \dot{\mathbf{x}}^{(j_x)}(t_i) \right] + \sum_{j_y=1}^{M_y} \mathbb{E} \left[\sup_{\dot{\mathbf{y}}^{(j_y)} \in \mathcal{W}^{P,2}} \frac{1}{N} \sum_{i=1}^N \epsilon_{ij_y} \dot{\mathbf{y}}^{(j_y)}(t_i) \right] \\
& \quad + \sum_{j_z=1}^{M_z} \mathbb{E} \left[\sup_{\dot{\mathbf{z}}^{(j_z)} \in \mathcal{W}^{P,2}} \frac{1}{N} \sum_{i=1}^N \epsilon_{ij_z} \dot{\mathbf{z}}^{(j_z)}(t_i) \right] \\
& \lesssim CMN^{-1/2}, \tag{Lemma 4}
\end{aligned}$$

where the last inequality comes from the fact that $\|(\dot{\mathbf{x}}, \dot{\mathbf{y}}, \dot{\mathbf{z}})\|_{\mathcal{W}_M^{P,2}} \leq C$ implies that $\|\dot{\mathbf{x}}^{(m)}\|_{\mathcal{W}^{P,2}}, \|\dot{\mathbf{y}}^{(m)}\|_{\mathcal{W}^{P,2}}, \|\dot{\mathbf{z}}^{(m)}\|_{\mathcal{W}^{P,2}} \leq C$ for all m . An analogous proof holds for $\widehat{\mathcal{R}}(\int \mathbb{F}_M^C)$. \square

Lemma 6. Denote M and $\mathcal{W}_M^{P,2}$ as in Lemma 2. For any $(\dot{\mathbf{x}}, \dot{\mathbf{y}}, \dot{\mathbf{z}}) \in \mathcal{W}_M^{P,2}$, $\hat{\mathbf{y}}_0 \in \mathbb{R}^{M_y}$, $\hat{\mathbf{z}}_0 \in \mathbb{R}^{M_z}$, define the differential equation error function

$$\begin{aligned}
e_{\dot{\mathbf{x}}, \dot{\mathbf{y}}, \dot{\mathbf{z}}, \hat{\mathbf{y}}_0, \hat{\mathbf{z}}_0}(\cdot) & := \left\| \begin{bmatrix} \dot{\mathbf{x}}(\cdot) - \mathbf{F}(\mathbf{x}, \mathbf{y}, \mathbf{z}) \\ \dot{\mathbf{y}}(\cdot) - \mathbf{G}(\mathbf{x}, \mathbf{y}, \mathbf{z}) \\ \mathbf{H}(\mathbf{x}, \mathbf{y}, \mathbf{z}) \end{bmatrix} \right\|_{\infty} \\
\mathbf{x}(t) & := \mathbf{x}_0 + \int_0^t \dot{\mathbf{x}}(\tau) d\tau, \quad \mathbf{y}(t) := \hat{\mathbf{y}}_0 + \int_0^t \dot{\mathbf{y}}(\tau) d\tau, \quad \mathbf{z}(t) := \hat{\mathbf{z}}_0 + \int_0^t \dot{\mathbf{z}}(\tau) d\tau,
\end{aligned} \tag{17}$$

For any $0 < C < \infty$, define $\mathbb{G}^{C,K}$ as the set of error functions

$$\left\{ e_{\dot{\mathbf{x}}, \dot{\mathbf{y}}, \dot{\mathbf{z}}, \hat{\mathbf{y}}_0, \hat{\mathbf{z}}_0}(\cdot) : \|(\dot{\mathbf{x}}, \dot{\mathbf{y}}, \dot{\mathbf{z}})\|_{\mathcal{W}_M^{P,2}} \leq C, \|\hat{\mathbf{y}}_0\|_{\infty} \leq K, \|\hat{\mathbf{z}}_0\|_{\infty} \leq K \right\}.$$

Then every error function in $\mathbb{G}^{C,K}$ is bounded by some constant \tilde{C} and $\widehat{\mathcal{R}}(\mathbb{G}^{C,K}) \lesssim CN^{-1/2}$.

Proof. Note that each error function in $\mathbb{G}^{C,K}$ is a Lipschitz function ($\|\cdot\|_{\infty}$), each of which is applied to the summation of two sub-functions:

1. a vector-valued RKHS function $((\dot{\mathbf{x}}(\cdot), \dot{\mathbf{y}}(\cdot), \dot{\mathbf{z}}(\cdot)))$ with norm less than C (i.e. an element of \mathbb{F}_M^C , as defined in Lemma 5), and
2. Lipschitz functions $(\mathbf{F}, \mathbf{G}, \mathbf{H})$ applied to the integral of a vector-valued RKHS function $(\dot{\mathbf{x}}, \dot{\mathbf{y}}, \dot{\mathbf{z}})$ with norm less than C (i.e. a Lipschitz function applied to an element of $\int \mathbb{F}_M^C$, as defined in Lemma 5).

Boundedness of the error functions falls from the fact $(\mathbf{x}, \mathbf{y}, \mathbf{z})$ are bounded, $\hat{\mathbf{y}}_0, \hat{\mathbf{z}}_0$ are bounded, and $\mathbf{F}, \mathbf{G}, \mathbf{H}$ are continuous (and thus bounded over $[0, T]$). The Rademacher complexity falls from standard Lipschitz and summation rules: $\widehat{\mathcal{R}}(\mathbb{G}^{C,K}) \lesssim \widehat{\mathcal{R}}(\mathbb{F}_M^C) + \widehat{\mathcal{R}}(\int \mathbb{F}_M^C) \lesssim CMN^{-1/2}$. \square

Now we are ready to prove Theorem 1.

Proof of Theorem 1. We begin by noting that

$$\begin{aligned}
B & := \inf_{(\mathbf{x}, \mathbf{y}, \mathbf{z}) \in \mathbb{S}} \sum_{m=1}^{M_x} |\hat{\mathbf{x}}^{(m)}|_{\mathcal{H}}^2 + \sum_{m=1}^{M_y} |\hat{\mathbf{y}}^{(m)}|_{\mathcal{H}}^2 + \sum_{m=1}^{M_z} |\hat{\mathbf{z}}^{(m)}|_{\mathcal{H}}^2 \\
& \asymp \inf_{(\mathbf{x}, \mathbf{y}, \mathbf{z}) \in \mathbb{S}} \|(\dot{\mathbf{x}}, \dot{\mathbf{y}}, \dot{\mathbf{z}})\|_{\mathcal{W}_M^{P,2}} < \infty
\end{aligned}$$

is implied by Lemma 1. (The equivalence in norms is given by combining the definition of $\mathcal{W}_M^{P,2}$ in Lemma 2 with the equivalence between Matérn and Sobolev spaces.) Let $(\mathbf{x}^*, \mathbf{y}^*, \mathbf{z}^*)$ be some element in \mathbb{S} that achieves this infimum (the existence of which is guaranteed by Lemma 3). We know that $\|(\hat{\mathbf{x}}_N, \hat{\mathbf{y}}_N, \hat{\mathbf{z}}_N)\|_{\mathcal{W}_M^{P,2}} \leq \|(\mathbf{x}^*, \mathbf{y}^*, \mathbf{z}^*)\|_{\mathcal{W}_M^{P,2}} = B$ —since $(\mathbf{x}^*, \mathbf{y}^*, \mathbf{z}^*)$ satisfies the constraints for Eq. (7)—and thus $(\hat{\mathbf{x}}_N, \hat{\mathbf{y}}_N, \hat{\mathbf{z}}_N) \in \mathbb{F}_M^B$ (as defined by Lemma 5).

Defining $e_{\hat{\mathbf{x}}_N, \hat{\mathbf{y}}_N, \hat{\mathbf{z}}_N, \hat{\mathbf{y}}_0, \hat{\mathbf{z}}_0}(\cdot)$ as in Lemma 6, we have that $e_{\hat{\mathbf{x}}_N, \hat{\mathbf{y}}_N, \hat{\mathbf{z}}_N, \hat{\mathbf{y}}_0, \hat{\mathbf{z}}_0}(t_i) = 0$ for each t_i in \mathcal{D} . Applying a standard uniform large law argument [e.g. 46, Thm. 4.2] we have that, for any $\delta > 0$,

$$\begin{aligned} \int_0^T e_{\hat{\mathbf{x}}_N, \hat{\mathbf{y}}_N, \hat{\mathbf{z}}_N, \hat{\mathbf{y}}_0, \hat{\mathbf{z}}_0}(\tau) d\tau &= \left| \frac{1}{N} \sum_{i=1}^N e_{\hat{\mathbf{x}}_N, \hat{\mathbf{y}}_N, \hat{\mathbf{z}}_N, \hat{\mathbf{y}}_0, \hat{\mathbf{z}}_0}(t_i) - \int_0^T e_{\hat{\mathbf{x}}_N, \hat{\mathbf{y}}_N, \hat{\mathbf{z}}_N, \hat{\mathbf{y}}_0, \hat{\mathbf{z}}_0}(\tau) d\tau \right| \\ &\leq 2\mathbb{E}_{t_i} \left[\widehat{\mathcal{R}}(\mathbb{G}^{B,K}) \right] + \delta \end{aligned}$$

with probability $1 - 2\exp(-\frac{N\delta^2}{8\tilde{C}^2})$ (where \tilde{C} is the constant defined in Lemma 6). Since $\widehat{\mathcal{R}}(\mathbb{G}^{B,K}) \lesssim BMN^{-1/2}$ (Lemma 6), we have that $\int_0^T e_{\hat{\mathbf{x}}_N, \hat{\mathbf{y}}_N, \hat{\mathbf{z}}_N, \hat{\mathbf{y}}_0, \hat{\mathbf{z}}_0}(\tau) d\tau \xrightarrow{\text{a.s.}} 0$, which implies that $\lim_{N \rightarrow \infty} (\hat{\mathbf{x}}_N, \hat{\mathbf{y}}_N, \hat{\mathbf{z}}_N)$ satisfies the differential equation almost everywhere.

Define $(\dot{\mathbf{x}}, \dot{\mathbf{y}}, \dot{\mathbf{z}})$ as the continuously-differentiable representative of $\lim_{N \rightarrow \infty} (\hat{\mathbf{x}}_N, \hat{\mathbf{y}}_N, \hat{\mathbf{z}}_N)$ (see [e.g. 9, Thm. 8.2]). Since $(\dot{\mathbf{x}}, \dot{\mathbf{y}}, \dot{\mathbf{z}})$ is continuously-differentiable and satisfies the differential equation everywhere, it must also be an element of \mathbb{S} . All together, this implies that $\|(\dot{\mathbf{x}}, \dot{\mathbf{y}}, \dot{\mathbf{z}})\|_{\mathcal{W}_M^{P,2}} \geq B$, and so $\|(\dot{\mathbf{x}}, \dot{\mathbf{y}}, \dot{\mathbf{z}})\|_{\mathcal{W}_M^{P,2}} = \|\lim_{N \rightarrow \infty} (\hat{\mathbf{x}}_N, \hat{\mathbf{y}}_N, \hat{\mathbf{z}}_N)\|_{\mathcal{W}_M^{P,2}} = B$. \square

C Robustness Checks and Variations

C.1 Sparse training data and data efficiency

The cardinality of the training set, \mathcal{D} , becomes an impediment in higher dimensions, where we have many state and jump variables. Therefore, it is crucial that we can obtain accurate approximate solutions with a sparse training data.

Fig. 4 shows the result of the Neoclassical Growth model (i.e., Eqs. (13) and (14)) solved with the Matérn kernel for sparse training data, $\mathcal{D} := 1, 5, 10, 15, 20, 25, 30$. The top-left panel shows the approximate and benchmark capital paths, denoted by $\hat{x}(t)$ and $x(t)$, respectively. The top-right panel shows the relative errors between the approximate and benchmark solutions for capital, denoted by $\varepsilon_x(t)$. The bottom-left panel shows the approximate and benchmark consumption paths, denoted by $\hat{y}(t)$ and $y(t)$, respectively. The bottom-right panel shows the relative errors between the approximate and benchmark solutions for consumption, denoted by $\varepsilon_y(t)$.

These results show that one can obtain very accurate approximate solution, even with a very sparse training data.

C.2 Robustness to the choice of the kernel and kernel parameters

Table 1 shows the result of the approximate solution of the Neoclassical Growth model, described in Eqs. (13) and (14)), for different Matérn kernels and kernel parameters.

The first three rows show the performance of the approximate solutions for three different kernels. We report the maximum and minimum of the absolute value of relative errors for both the capital path, $\hat{x}(t)$, and the consumption path, $\hat{y}(t)$. The first row presents the baseline solution, Matérn kernel with $\nu = \frac{1}{2}$. The second row shows results for Matérn kernel with $\nu = \frac{3}{2}$, defined as

$$K(t_i, t_j) = C_{\frac{3}{2}}(t_i, t_j) = \sigma^2 \left(1 + \frac{\sqrt{3}|t_i - t_j|}{\ell} \right) \exp \left(-\frac{\sqrt{3}|t_i - t_j|}{\ell} \right),$$

and the third row for $\nu = \frac{5}{2}$, defined as

$$K(t_i, t_j) = C_{\frac{5}{2}}(t_i, t_j) = \sigma^2 \left(1 + \frac{\sqrt{5}|t_i - t_j|}{\ell} + \frac{5|t_i - t_j|^2}{3\ell^2} \right) \exp \left(-\frac{\sqrt{5}|t_i - t_j|}{\ell} \right).$$

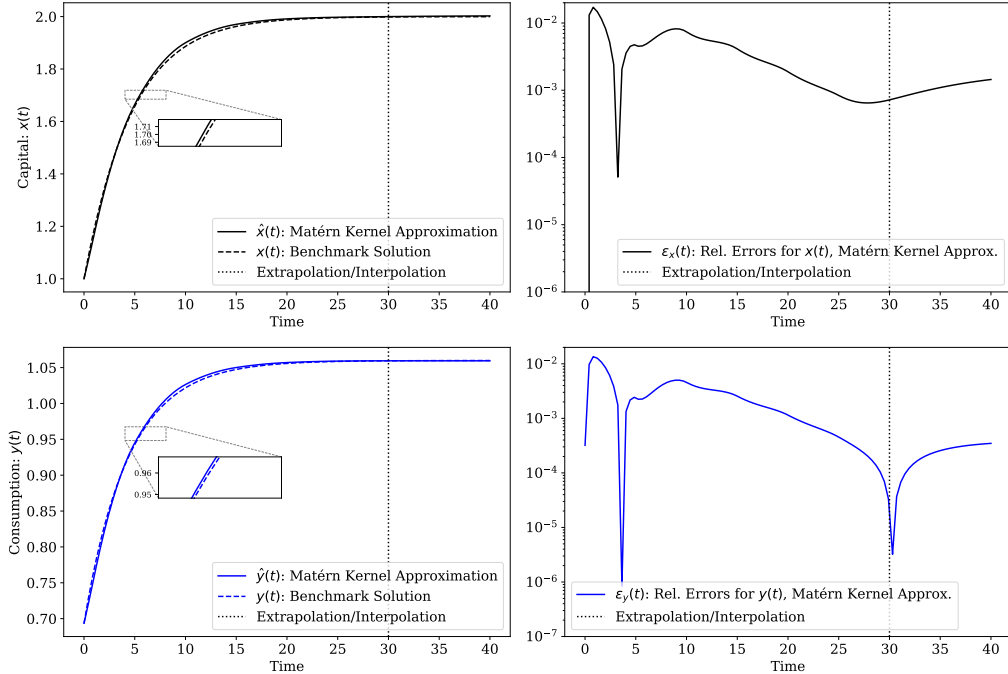


Figure 4: The Neoclassical Growth model (i.e., Eqs. (13) and (14)) solved using the Matérn kernel for a sparse training data. The top-left panel shows the approximate and benchmark capital paths. The top-right panel shows the relative errors between the approximate and benchmark solutions for capital. The bottom-left panel shows the approximate and benchmark consumption paths. The bottom-right panel shows the relative errors between the approximate and benchmark solutions for consumption. Accurate solutions can be obtained even with sparse training data.

ν	ℓ	Max of Rel. Error: $\hat{x}(t)$	Max of Rel. Error: $\hat{y}(t)$	Min of Rel. Error: $\hat{x}(t)$	Min of Rel. Error: $\hat{y}(t)$
1/2	10	2.3e-03	5.9e-04	1.5e-04	6.5e-07
3/2	10	5.1e-04	3.3e-04	1.5e-06	9.7e-07
5/2	10	1.0e-04	9.0e-05	2.7e-05	5.7e-08
1/2	2	4.1e-03	2.6e-03	3.0e-04	8.0e-06
1/2	20	4.2e-03	1.1e-03	1.8e-04	2.3e-06

Table 1: The robustness of the approximate solutions of the Neoclassical Growth model (i.e., Eqs. (13) and (14)) is tested using different Matérn kernels, $\nu = \frac{1}{2}, \frac{3}{2}, \frac{5}{2}$, and length scales $\ell = 2, 20$. We report the maximum and minimum of the absolute value of relative errors for both the capital path, $\hat{x}(t)$, and the consumption path, $\hat{y}(t)$. Our method is not sensitive to the choice of Matérn kernels and length scales.

The last two rows show the performance of the approximate solutions for two different *length scales*, $\ell = 2$ and $\ell = 20$.

Throughout these experiments, we achieve highly accurate approximate solutions. Therefore, the results demonstrate insensitivity to the selection of Matérn kernels and the length scales.

C.3 Smaller time horizons: accurate short-run dynamics

One might suspect that achieving an accurate optimal solution, which does not violate the transversality condition, Eq. (15), is only possible if one uses a large time horizon in the training data. For instance, we use $\mathcal{D} = 0, 1, 2, \dots, 30$ to obtain the results depicted in Fig. 2. In this experiment, we establish that we can still achieve accurate short-run dynamics by using a smaller time horizon.

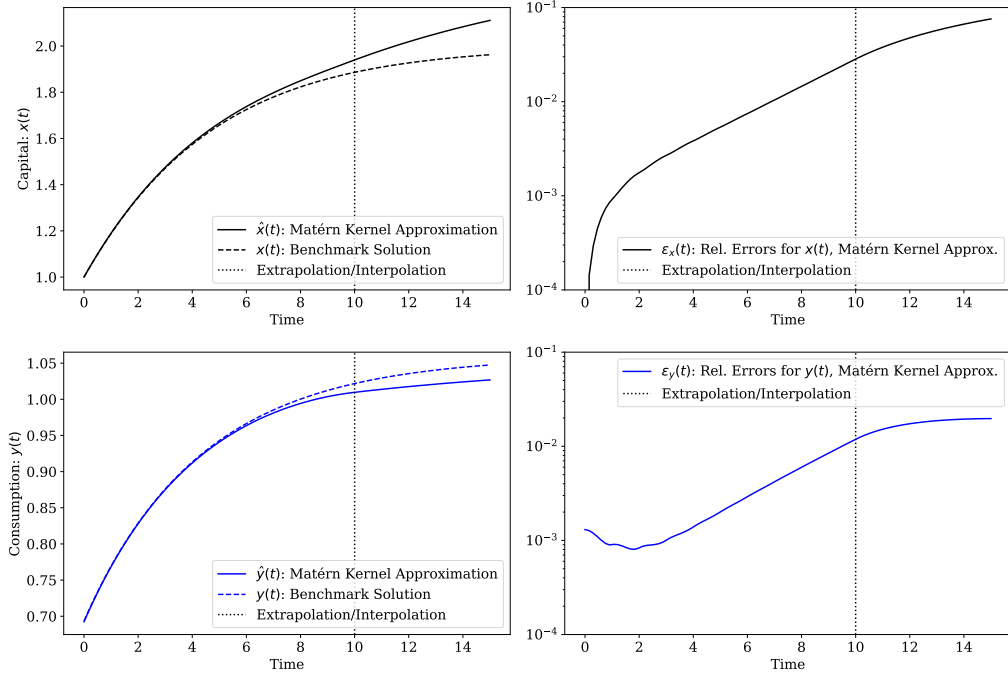


Figure 5: The Neoclassical Growth model (i.e., Eqs. (13) and (14)) solved with Matérn kernel for training data with a smaller time horizon. The top-left panel shows the approximate and benchmark capital paths. The top-right panel shows the relative errors between the approximate and benchmark solutions for capital. The bottom-left panel shows the approximate and benchmark consumption paths. The bottom-right panel shows the relative errors between the approximate and benchmark solutions for consumption. Very accurate short-run dynamics can be obtained with training data using a smaller time horizon.

Fig. 5 shows the approximate solutions for the Neoclassical Growth model (i.e., Eqs. (13) and (14)) for training data with smaller time horizon, defined as $\mathcal{D} := \{0, 1, 2, \dots, 10\}$. The top-left panel shows the approximate and benchmark capital paths, denoted by $\hat{x}(t)$ and $x(t)$, respectively. The top-right panel shows the relative errors between the approximate and benchmark solutions for capital, denoted by $\varepsilon_x(t)$. The bottom-left panel shows the approximate and benchmark consumption paths, denoted by $\hat{y}(t)$ and $y(t)$, respectively. The bottom-right panel shows the relative errors between the approximate and benchmark solutions for consumption, denoted by $\varepsilon_y(t)$.

C.4 Neoclassical Growth model: differential-algebraic equations

In this section, we solve a different formulation of the problem introduced in section 4.2. Introducing a *static* variable, $z(t) \in \mathbb{R}$, defined as

$$z(t) := f'(x(t)) - \delta,$$

we can reformulate Eqs. (13) and (14) in the following way

$$\dot{\mathbf{x}}(t) = f(\mathbf{x}(t)) - \mathbf{y}(t) - \delta \mathbf{x}(t), \quad (18)$$

$$\dot{\mathbf{y}}(t) = \mathbf{y}(t) [z(t) - r], \quad (19)$$

$$0 = z(t) - f'(x(t)) + \delta, \quad (20)$$

where $f(x) = x^a$, $f'(x) = ax^{a-1}$, and the transversality condition, Eq. (15) remains unchanged. The static variable, $z(t)$, represents the real interest rate in this economy.

What distinguishes this example from the Neoclassical Growth model is the presence of an algebraic equation, Eq. (20), in the equations. Formally, using the notation introduced in Eq. (3)

$$\mathbf{H}(\mathbf{x}(t), \mathbf{y}(t), z(t)) := z(t) - f'(x(t)) + \delta.$$

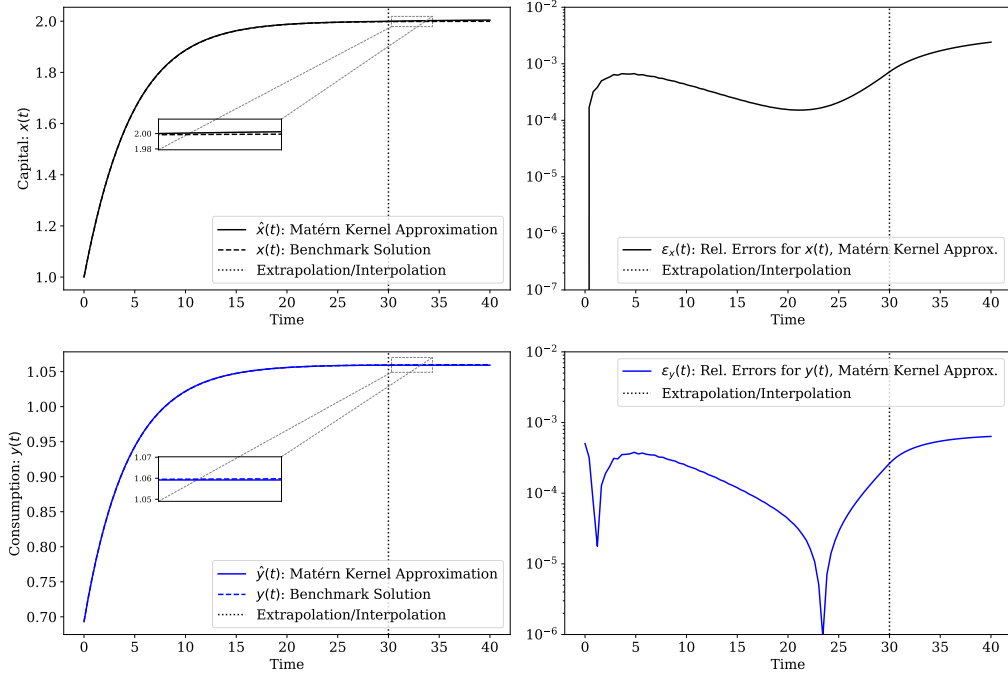


Figure 6: DAE formulation of the Neoclassical Growth model (i.e., Eqs. (18) and (20)) solved with Matérn kernel. The top-left panel shows the approximate and benchmark capital paths. The top-right panel shows the relative errors between the approximate and benchmark solutions for capital. The bottom-left panel shows the approximate and benchmark consumption paths. The bottom-right panel shows the relative errors between the approximate and benchmark solutions for consumption. Accurate approximate solutions can be obtained for the DAE formulation.

In this example, we aim to investigate whether our method can handle differential-algebraic equations.

Using $\hat{\mathbf{x}}(t) = \mathbf{x}_0 + \int_0^t \hat{\mathbf{x}}(\tau) d\tau$, $\hat{\mathbf{y}}(t) = \hat{\mathbf{y}}_0 + \int_0^t \hat{\mathbf{y}}(\tau) d\tau$, and $\hat{\mathbf{z}}(t) = \hat{\mathbf{z}}_0 + \int_0^t \hat{\mathbf{z}}(\tau) d\tau$, we solve the following optimization

$$\begin{aligned} \min_{\hat{\mathbf{x}}, \hat{\mathbf{y}}, \hat{\mathbf{z}}, \hat{\mathbf{y}}_0, \hat{\mathbf{z}}_0} \quad & \|\dot{\hat{\mathbf{x}}}\|_{\mathcal{H}}^2 + \|\dot{\hat{\mathbf{y}}}\|_{\mathcal{H}}^2 + \|\dot{\hat{\mathbf{z}}}\|_{\mathcal{H}}^2 \\ \text{s.t.} \quad & \dot{\hat{\mathbf{x}}}(t_i) = f(\hat{\mathbf{x}}(t_i)) - \hat{\mathbf{y}}(t_i) - \delta \hat{\mathbf{x}}(t_i), \quad \text{for all } t_i \in \mathcal{D}, \\ & \dot{\hat{\mathbf{y}}}(t_i) = \hat{\mathbf{g}}(t_i) [\hat{\mathbf{z}}(t_i) - r], \quad \text{for all } t_i \in \mathcal{D}, \\ & 0 = \hat{\mathbf{z}}(t_i) - f'(\hat{\mathbf{x}}(t_i)) + \delta, \quad \text{for all } t_i \in \mathcal{D}, \end{aligned}$$

to obtain approximate solutions for x , y , and z .

Here, $\|\dot{\hat{\mathbf{x}}}\|_{\mathcal{H}}^2 = \boldsymbol{\alpha}^x \top K \boldsymbol{\alpha}^x$, $\|\dot{\hat{\mathbf{y}}}\|_{\mathcal{H}}^2 = \boldsymbol{\alpha}^y \top K \boldsymbol{\alpha}^y$, and $\|\dot{\hat{\mathbf{z}}}\|_{\mathcal{H}}^2 = \boldsymbol{\alpha}^z \top K \boldsymbol{\alpha}^z$. We use the same numerical values introduced in section 4.2.

Fig. 6 shows the approximate solutions of the DAE formulation of the Neoclassical Growth model for the training data $\mathcal{D} = \{0, 1, \dots, 30\}$. The top-left panel shows the approximate and benchmark capital paths, denoted by $\hat{x}(t)$ and $x(t)$, respectively. The top-right panel shows the relative errors between the approximate and benchmark solutions for capital, denoted by $\varepsilon_x(t)$. The bottom-left panel shows the approximate and benchmark consumption paths, denoted by $\hat{y}(t)$ and $y(t)$, respectively. The bottom-right panel shows the relative errors between the approximate and benchmark solutions for consumption, denoted by $\varepsilon_y(t)$.

This result establishes that our method can find accurate approximate solutions for the DAE formulation of the Neoclassical Growth model.

D More Applications

In this section, we provide more applications in economics and business. Each application differs fundamentally from the problems introduced in Sec. 4. In Appx. D.1, we solve a model that incorporates the time evolution of human capital and its interaction with physical capital in economic growth. This model has five variables: two state variables and three jump variables. In Appx. D.2, we solve an optimal advertising model. This model is considered a building block of modern dynamic advertising in business economics and operations management.

D.1 Human capital and growth

In this example, we solve the Neoclassical Growth model with human and physical capital as illustrated in [1]. The optimal paths $\mathbf{x}_k(t)$, $\mathbf{x}_h(t)$, $\mathbf{y}_c(t)$, $\mathbf{y}_k(t)$, $\mathbf{y}_h(t)$, solve

$$\dot{\mathbf{x}}_k(t) = \mathbf{y}_k(t) - \delta_k \mathbf{x}_k(t), \quad (21)$$

$$\dot{\mathbf{x}}_h(t) = \mathbf{y}_h(t) - \delta_h \mathbf{x}_h(t), \quad (22)$$

$$\dot{\mathbf{y}}_c(t) = \mathbf{y}_c(t) [f_1(\mathbf{x}_k(t), \mathbf{x}_h(t)) - \delta_k - r], \quad (23)$$

$$0 = f(\mathbf{x}_k(t), \mathbf{x}_h(t)) - \mathbf{y}_c(t) - \mathbf{y}_k(t) - \mathbf{y}_h(t), \quad (24)$$

$$0 = f_2(\mathbf{x}_k(t), \mathbf{x}_h(t)) - f_1(\mathbf{x}_k(t), \mathbf{x}_h(t)) + \delta_k - \delta_h, \quad (25)$$

for given initial conditions $\mathbf{x}_k(0) = \mathbf{x}_{k_0}$, $\mathbf{x}_h(0) = \mathbf{x}_{h_0}$, and two transversality conditions

$$0 = \lim_{t \rightarrow \infty} e^{-rt} \frac{\mathbf{x}_k(t)}{\mathbf{y}_c(t)}, \quad (26)$$

$$0 = \lim_{t \rightarrow \infty} e^{-rt} \frac{\mathbf{x}_h(t)}{\mathbf{y}_c(t)}. \quad (27)$$

The production function is defined as $f(\mathbf{x}_k(t), \mathbf{x}_h(t)) = \mathbf{x}_k(t)^{a_k} \mathbf{x}_h(t)^{a_h}$. Here, $f_1(\cdot, \cdot)$ is the derivative with respect to the first input and $f_2(\cdot, \cdot)$ is the derivative with respect to the second input. The two constants in the production function, a_k and a_h , are positive numbers, such that $a_k + a_h < 1$. Additionally, $\delta_k > 0$, $\delta_h > 0$, and $r > 0$.

Human capital is denoted by $\mathbf{x}_h(t)$, physical capital by $\mathbf{x}_k(t)$, consumption by $\mathbf{y}_c(t)$, investment in human capital by $\mathbf{y}_h(t)$, and investment in physical capital by $\mathbf{y}_k(t)$. Here $\mathbf{y}_c(t)$, $\mathbf{y}_h(t)$, and $\mathbf{y}_k(t)$ are the jump variables. The state variables are $\mathbf{x}_h(t)$ and $\mathbf{x}_k(t)$.

This problem is more challenging than the Neoclassical Growth model introduced in Sec. 4 because it is high-dimensional and involves two algebraic equations, Eqs. (24) and (25).

Using $\hat{\mathbf{x}}_k(t) = \mathbf{x}_{k_0} + \int_0^t \hat{\mathbf{x}}_k(\tau) d\tau$, $\hat{\mathbf{x}}_h(t) = \mathbf{x}_{h_0} + \int_0^t \hat{\mathbf{x}}_h(\tau) d\tau$, $\hat{\mathbf{y}}_c(t) = \hat{\mathbf{y}}_{c_0} + \int_0^t \hat{\mathbf{y}}_c(\tau) d\tau$, $\hat{\mathbf{y}}_h(t) = \hat{\mathbf{y}}_{h_0} + \int_0^t \hat{\mathbf{y}}_h(\tau) d\tau$, $\hat{\mathbf{y}}_k(t) = \hat{\mathbf{y}}_{k_0} + \int_0^t \hat{\mathbf{y}}_k(\tau) d\tau$, we solve the following optimization

$$\begin{aligned} \min_{\hat{\mathbf{x}}_k, \hat{\mathbf{x}}_h, \hat{\mathbf{y}}_c, \hat{\mathbf{y}}_h, \hat{\mathbf{y}}_k, \hat{\mathbf{y}}_{c_0}, \hat{\mathbf{y}}_{h_0}, \hat{\mathbf{y}}_{k_0}} \quad & \|\hat{\dot{\mathbf{x}}}_k\|_{\mathcal{H}}^2 + \|\hat{\dot{\mathbf{x}}}_h\|_{\mathcal{H}}^2 + \|\hat{\dot{\mathbf{y}}}_c\|_{\mathcal{H}}^2 + \|\hat{\dot{\mathbf{y}}}_h\|_{\mathcal{H}}^2 + \|\hat{\dot{\mathbf{y}}}_k\|_{\mathcal{H}}^2 \\ \text{s.t.} \quad & \hat{\dot{\mathbf{x}}}_k(t_i) = \hat{\mathbf{y}}_k(t_i) - \delta_k \hat{\mathbf{x}}_k(t_i), \quad \text{for all } t_i \in \mathcal{D}, \\ & \hat{\dot{\mathbf{x}}}_h(t_i) = \hat{\mathbf{y}}_h(t_i) - \delta_h \hat{\mathbf{x}}_h(t_i), \quad \text{for all } t_i \in \mathcal{D}, \\ & \hat{\dot{\mathbf{y}}}_c(t_i) = \hat{\mathbf{y}}_c(t_i) [f_1(\hat{\mathbf{x}}_k(t_i), \hat{\mathbf{x}}_h(t_i)) - \delta_k - r], \quad \text{for all } t_i \in \mathcal{D}, \\ & 0 = f(\hat{\mathbf{x}}_k(t_i), \hat{\mathbf{x}}_h(t_i)) - \hat{\mathbf{y}}_c(t_i) - \hat{\mathbf{y}}_k(t_i) - \hat{\mathbf{y}}_h(t_i), \quad \text{for all } t_i \in \mathcal{D}, \\ & 0 = f_2(\hat{\mathbf{x}}_k(t_i), \hat{\mathbf{x}}_h(t_i)) - f_1(\hat{\mathbf{x}}_k(t_i), \hat{\mathbf{x}}_h(t_i)) + \delta_k - \delta_h, \quad \text{for all } t_i \in \mathcal{D}, \end{aligned}$$

to obtain approximate solutions for $\mathbf{x}_k(t)$, $\mathbf{x}_h(t)$, $\mathbf{y}_c(t)$, $\mathbf{y}_k(t)$, $\mathbf{y}_h(t)$.

Here, $\|\hat{\dot{\mathbf{x}}}_k\|_{\mathcal{H}}^2 = \boldsymbol{\alpha}^{x_k \top} K \boldsymbol{\alpha}^{x_k}$, $\|\hat{\dot{\mathbf{x}}}_h\|_{\mathcal{H}}^2 = \boldsymbol{\alpha}^{x_h \top} K \boldsymbol{\alpha}^{x_h}$, $\|\hat{\dot{\mathbf{y}}}_c\|_{\mathcal{H}}^2 = \boldsymbol{\alpha}^{y_c \top} K \boldsymbol{\alpha}^{y_c}$, $\|\hat{\dot{\mathbf{y}}}_h\|_{\mathcal{H}}^2 = \boldsymbol{\alpha}^{y_h \top} K \boldsymbol{\alpha}^{y_h}$, and $\|\hat{\dot{\mathbf{y}}}_k\|_{\mathcal{H}}^2 = \boldsymbol{\alpha}^{y_k \top} K \boldsymbol{\alpha}^{y_k}$.

In this experiment we, use $\delta_k = 0.1$, $\delta_h = 0.05$, $\alpha_k = \frac{1}{3}$, $\alpha_h = \frac{1}{4}$, $r = 0.11$, $x_{k_0} = 1.5$, and $x_{h_0} = 1.37$ as the numerical values for the economic parameters. We use $\mathcal{D} = \{0, 1, \dots, 80\}$ as the training data.

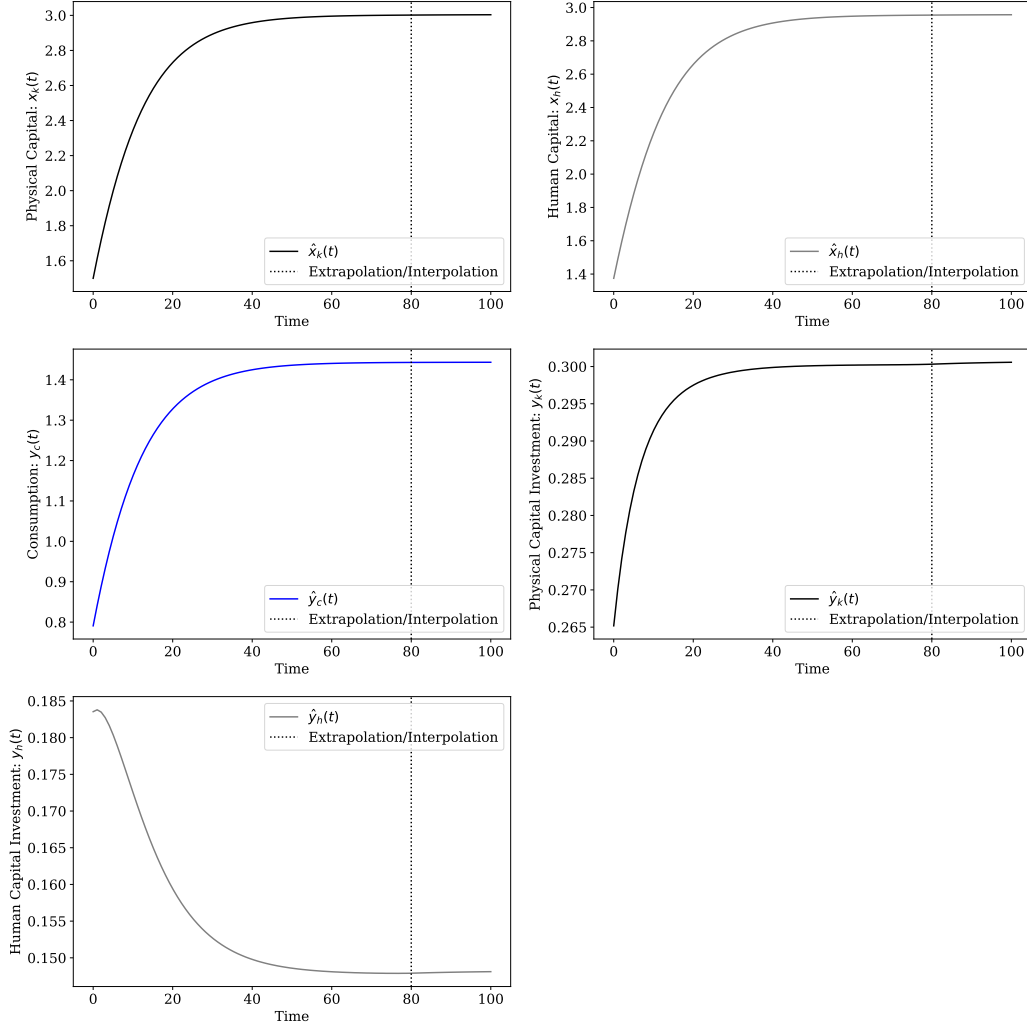


Figure 7: The Neoclassical Growth model with human capital (i.e., Eqs. (21) to (25)) is solved using the Matérn kernel for the training data $\mathcal{D} = \{0, 1, \dots, 80\}$. The top-left panel shows the approximate physical capital path. The top-right panel shows the approximate human capital path. The middle-left panel shows the approximate consumption paths. The middle-right panel shows the approximate investment in physical capital path. The bottom-left panel shows the approximate investment in human capital path. The approximate solutions demonstrate convergence to the correct set of steady states. Therefore, they satisfy the transversality conditions.

Fig. 7 shows the approximate physical capital path, denoted by $\hat{x}_k(t)$, the approximate human capital path, denoted by $\hat{x}_h(t)$, the approximate consumption path, denoted by $\hat{y}_c(t)$, the approximate investment in physical capital path, denoted by $\hat{y}_k(t)$, and the approximate investment in human capital path, denoted by $\hat{y}_h(t)$. The vertical dashed line shows the boundary between the interpolation and extrapolation regions.

This result establishes that even in higher dimensions with more complex algebraic equations, the approximate solutions converge to the correct set of steady states. Therefore, the solutions satisfy the transversality conditions.

The correct set of steady states. How do we know the approximate solutions converge to the correct set of steady states? A set of solutions that violates the transversality conditions is characterized by a consumption path that converges to zero, and human and physical capital paths that converge to finite but very large values. Hence, in this case, $\lim_{t \rightarrow \infty} e^{-rt} \frac{\mathbf{x}_k(t)}{\mathbf{y}_c(t)} = \lim_{t \rightarrow \infty} e^{-rt} \frac{\mathbf{x}_h(t)}{\mathbf{y}_c(t)} = \infty$.

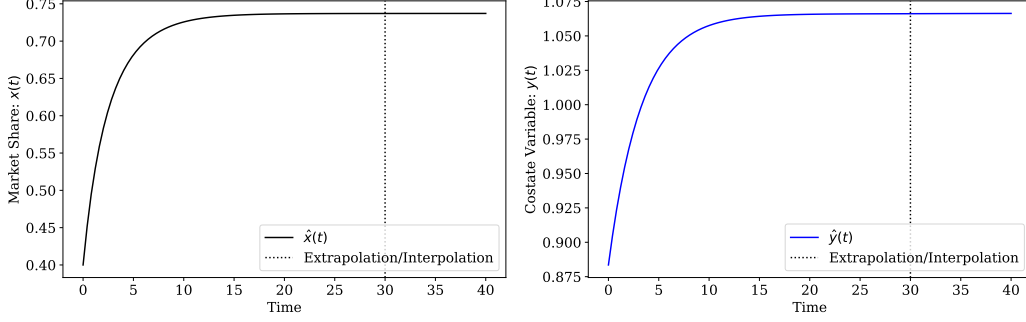


Figure 8: The Optimal Advertising model (i.e., Eqs. (28) to (29)) solved using the Matérn kernel for the training data $\mathcal{D} = \{0, 1, \dots, 30\}$. The left panel shows the approximate market share and the right panel shows the approximate costate variable. The approximate solutions demonstrate convergence to the correct set of steady states. Therefore, they satisfy the transversality condition.

Since the approximate solutions shown in Fig. 7 do not exhibit this behavior, we can be confident that they converge to the correct set of steady states.

D.2 Optimal Advertising

In this example we solve an optimal advertising model based on the classical model of expenditure on advertising introduced in [45]. The optimal paths $\mathbf{x}(t)$ and $\mathbf{y}(t)$, solve

$$\dot{\mathbf{x}}(t) = [1 - \mathbf{x}(t)]^{\frac{1}{1-\kappa}} [\kappa \mathbf{y}(t)]^{\frac{\kappa}{1-\kappa}} - \beta \mathbf{x}(t), \quad (28)$$

$$\dot{\mathbf{y}}(t) = -\gamma + (r + \beta) \mathbf{y}(t) + \mathbf{y}(t)^{\frac{1}{1-\kappa}} \left(\kappa [1 - \mathbf{x}(t)] \right)^{\frac{\kappa}{1-\kappa}} \quad (29)$$

for a given initial condition $\mathbf{x}(0) = \mathbf{x}_0$, and a transversality condition

$$\lim_{t \rightarrow \infty} e^{-rt} \mathbf{y}(t) = 0, \quad (30)$$

Here, \mathbf{x} is the market share of the company, and \mathbf{y} is the costate variable.

The parameter κ is a constant between 0 and 1, β is strictly positive, r is the discount rate, the constant γ is defined as $\gamma \equiv \frac{\beta+r}{c}$, and c is the cost of advertising. See [40, 47] for a detailed treatment of this problem.

Similar to the linear asset pricing model, the optimal advertising problem has a unique steady state, which is a saddle path. Consequently, any sub-optimal path diverges. However, unlike the linear asset pricing model, this is a two-dimensional problem, which makes finding the solution a more challenging task.

Using $\hat{\mathbf{x}}(t) = \mathbf{x}_0 + \int_0^t \hat{\mathbf{x}}(\tau) d\tau$ and $\hat{\mathbf{y}}(t) = \hat{\mathbf{y}}_0 + \int_0^t \hat{\mathbf{y}}(\tau) d\tau$ we solve the following optimization

$$\min_{\hat{\mathbf{x}}, \hat{\mathbf{y}}, \hat{\mathbf{y}}_0} \|\hat{\mathbf{x}}\|_{\mathcal{H}}^2 + \|\hat{\mathbf{y}}\|_{\mathcal{H}}^2$$

$$\text{s.t. } \hat{\mathbf{x}}(t_i) = [1 - \hat{\mathbf{x}}(t_i)]^{\frac{1}{1-\kappa}} [\kappa \hat{\mathbf{y}}(t_i)]^{\frac{\kappa}{1-\kappa}} - \beta \hat{\mathbf{x}}(t_i), \quad \text{for all } t_i \in \mathcal{D},$$

$$\hat{\mathbf{y}}(t_i) = -\gamma + (r + \beta) \hat{\mathbf{y}}(t_i) + \hat{\mathbf{y}}(t_i)^{\frac{1}{1-\kappa}} \left(\kappa [1 - \hat{\mathbf{x}}(t_i)] \right)^{\frac{\kappa}{1-\kappa}}, \quad \text{for all } t_i \in \mathcal{D},$$

to obtain approximate solutions for $\mathbf{x}(t)$ and $\mathbf{y}(t)$. Here, $\|\hat{\mathbf{x}}\|_{\mathcal{H}}^2 = \boldsymbol{\alpha}^x \top K \boldsymbol{\alpha}^x$, and $\|\hat{\mathbf{y}}\|_{\mathcal{H}}^2 = \boldsymbol{\alpha}^y \top K \boldsymbol{\alpha}^y$.

In this example we use $x_0 = 0.4$, $r = 0.11$, $c = 0.5$, $\beta = 0.05$, $\kappa = 0.5$, and $\gamma = \frac{\beta+r}{c} = 0.32$ as the numerical values for the parameters. We use $\mathcal{D} = \{0, 1, \dots, 30\}$ as the training data.

Fig. 8 shows the approximate market share, denoted by $\hat{x}(t)$ and the approximate costate variable, denoted by $\hat{y}(t)$. The vertical dashed line shows the boundary between the interpolation and extrapolation regions.

This result establishes that the approximate solutions demonstrate convergence to the correct set of steady states. Therefore, they satisfy the transversality condition.

The correct set of steady states. How do we know the approximate solutions converge to the correct set of steady states? As shown in Fig. 8, the approximate costate variable approaches a finite number. Therefore, $\lim_{t \rightarrow \infty} e^{-rt} \hat{y}(t) = 0$.